THE FLORIDA STATE UNIVERSITY

DEPARTMENT OF METEOROLOGY

MESOSCALE VARIABILITY OF SEA SURFACE TEMPERATURES

By
CLEVELAND G. HOLLADAY

A Thesis submitted to
the Department of Meteorology
in partial fulfillment of the
requirements for the degree of
Master of Science

Approved:

James J. O'Brien
Professor directing Thesis

Lawrence T. Gilbert

Robert Ellsworth

Charles Hosler

August, 1974

Charles Hosler

August, 1974

ABSTRACT

Results of an investigation of the nature of the mesoscale variability of SST in the upwelling zone off the central coast of Oregon are presented. A knowledge of the mesoscale variability of sea surface temperatures is important toward understanding the mesoscale air-sea interaction process in an upwelling zone. Almost-daily sea surface temperature data gathered by remote sensing techniques provided the basis for this investigation. These data were gathered over a period of sixty days during the COHO Project in summer, 1973. In order to study the influence of wind forcing on the mesoscale sea surface temperature field, wind data were gathered from an anemometer located at Newport, Oregon.

Some important results of this investigation are these: a) the daily sea surface temperature fields respond rapidly to wind forcing; b) the three-week mean sea surface temperatures tend to follow the large-scale bathymetry; c) identification of sea surface temperature eddies from day to day on daily perturbation (from the three-week means) maps is made difficult because of the existence of strong horizontal flow and strong shear in the longshore current. Other important results are revealed by a two-dimensional spectral analysis of the daily horizontal sea surface temperature fields and the perturbation fields. This analysis indicates that a large amount of variance of the sea surface temperature is concentrated in the 16-40 km wavelength range, and over the
sis indicates that a large amount of variance of the sea surface temperature is concentrated in the 16-40 km wavelength range, and over the
range of scales from 4-20 km the isotropic part of the temperature

variance spectrum obeys a -3 power law. These spectral results are important biologically and physically. An interesting feature of the mesoscale SST field, which is also important biologically and physically, is the existence of strong horizontal sea surface temperature gradients called "oceanic fronts."

ACKNOWLEDGMENTS

The author wishes to acknowledge the support of the Office for International Decade of Ocean Exploration (IDOE) for their sponsorship of the CORC Project. Funds to operate the project were supplied by NOAA Grant No. 04-3-022-28. This work was also supported by IDOE through the Coastal Upwelling Ecosystems Analysis (CUEA) Program under NSF Grant No. GX-33502. The Office of Naval Research, Ocean Science and Technology Division, provided partial support. Computations were performed on the CDC 6500 computer at the Florida State University, Tallahassee.

It is with much admiration and respect that I extend my appreciation to my major professor, Dr. James J. O'Brien, for his suggestions and criticisms during the course of this work. Dr. T. A. Gleason, Dr. S. L. Hess, Dr. C. L. Jordan, Dr. R. F. D. Perret, and Dr. J. J. Stephens deserve many thanks for their consultation and suggestions. I am especially indebted to helpful suggestions given to me during the course of this work by Dr. J. D. Thompson and Dr. H. E. Hurlburt. My appreciation is extended to the members of the Mesoscale Atmospheric Oceanic Interaction Research Group directed by Dr. James J. O'Brien for their helpful suggestions and encouragement throughout my graduate career. I extend special thanks to James Merritt who helped me with much of the computer programming involved in the data reduction and analysis, and also to Jim Clary who helped me with computer programming involved in the spectral analysis. Thanks are also due to Richard Berler, Paul Duval, Terry Moore, Robert Rigy, Bob Ortiz, Bob Shaw, and Ken Remington who helped in digitizing the

sea surface temperature data. Thanks are also due to Dewey Rudd for drafting most of the figures. I am grateful to Caroline Williams, and my sister, Margaret Holladay, for their cheerful willingness to type my early draft versions of the manuscript, and especially to Mrs. Gerry Woodhouse who was responsible for typing the final copy.

TABLE OF CONTENTS

LIST OF TABLES

LIST OF ILLUSTRATIONS

List of Illustrations - continued

List of Illustrations - continued

List of Illustrations - continued

Figure | Page

I. INTRODUCTION

One of the intriguing characteristics of a coastal upwelling zone is the mesoscale variability of the observed sea surface temperatures. A knowledge of the mesoscale spatial scales of the SST (sea surface temperatures) is important toward understanding the mesoscale air-sea interaction process in an upwelling zone. (A conclusion from the International Coordinating Committee for CINECA [1971] is that "the sea surface temperature is the most important single-parameter which can indicate areas of upwelling.") Investigators (e.g., Smith, 1968) have long known that along the eastern boundaries of oceans low surface temperatures often occur due to upwelling of cooler subsurface water. In the Northern Hemisphere an equatorward wind stress along the eastern boundary of an ocean combined with the effect of the earth's rotation produces a mass transport offshore in a surface Ekman layer. This divergence of surface waters away from the coast results in a cold water being upwelled from the subsurface layers to replace this offshore flowing water mass. July and August are months of intense upwelling off the coast of Oregon (Bakun, 1972). During these months sea surface temperatures observed within a few kilometers of shore may be as much as 8C cooler than SST seaward of the shelf edge (about 30 km). This difference in winter is rarely more than 1C. The annual range of SST along the Oregon coast is less than 3C due to summer upwelling (Smith, 1968). We shall, however, document daily changes greater than 3C. From the

climatological, ecological, and physical standpoints, coastal upwelling is an important oceanic phenomenon. The depression of SST by upwelling may act as a constraint on atmospheric convection and evaporation. The occurrence of upwelling also contributes to increased biological productivity of the sea. It is estimated that over half of the food for the earth's fish is produced in upwelling regions (Ryther, 1969).

In this paper some of the results of an investigation of the nature of this mesoscale variability of SST off the central coast of Oregon will be presented. Almost-daily sea surface temperature data, which were gathered over a period of sixty days during the COHO Project in summer, 1973, provided the basis for this investigation. This project was undertaken to study the feasibility of predicting environmental conditions favorable for the location of Coho Salmon. Upwelling off the coast of Oregon was studied intensively during the summer months of 1972 and 1973 by scientists participating in Coastal Upwelling Experiment phases I and II (CUE-I and CUE-II) of which the COHO Project was a part.

Important to the understanding of the mesoscale variability of SST is a knowledge of the large-scale wind field in the region that the SST were gathered. The upwelling season off the coast of Oregon has a time scale of several months. Generally, though, northerly winds do not blow steadily during this whole period. Instead, CUE researchers observed "upwelling events" which occurred on the time scale of days or weeks. During these events winds are generally from the north and northwest. This variability in wind forcing seems responsible for rapid

weeks. During these events winds are generally from the north and northwest. This variability in wind forcing seems responsible for rapid

changes in the SST field. Data from the COHO Project reveal that nearshore SST may drop as much as 6C in three days during periods of intense

northerly winds. CUE-I researchers found that during an upwelling event the warmest temperatures shoreward of the shelf edge may become cooler than the coldest temperatures in the region prior to the event, a result also shown by the COHO data (O'Brien, 1972).

Another interesting feature observed during CUE-I and II in the upwelling region off the coast of Oregon is that on certain days the SST field may have embedded in it regions of strong horizontal temperature gradients called "oceanic fronts." SST may change several degrees C within several hundred meters to a kilometer within one of these frontal zones. These fronts are rather well-defined and their location usually changes from day to day. The length of the frontal zone may vary from several kilometers to several tens of kilometers. These oceanic fronts may also intersect the coastline at some location and then extend seaward in a SSW or SW direction. Because they concentrate phytoplankton and other buoyant materials, these fronts are quite important biologically.

In order to broach the subject of the mesoscale variability of SST in an upwelling zone, a preview of some of the observed characteristics of the SST field has been presented above. Topics to be investigated in more detail later in this paper are: 1) the response of the SST field to wind forcing; 2) horizontal sea surface temperature gradients and their attendant oceanic fronts; 3) means and perturbations from means for periods of three weeks; 4) a spectral analysis to determine the scales of the eddies in the upwelling zone. Some of the important results from the consideration of these topics will be presented briefly in this introductory section.

We show that there is a strong correlation between the wind field and the SST field as mentioned earlier in this section. An analysis of the three-week means shows that the mean isotherms tend to follow the large-scale bathymetry of the upwelling region. Inspection of the daily perturbations from these means leads one to conclude that it is difficult to follow individual eddies from day to day. The reason for this is that the horizontal flow in this area is strong (10-40 cm sec^{-1}) and there is a strong shear in the longshore current (Garvine, 1974). The greatest daily variability of the mesoscale SST field is found in the first few kilometers near shore. Finally, results from the two-dimensional spectral analysis indicate that over the range of scales from 4-20 km the isotropic portion of the temperature variance spectrum $E_1(k)$ is shown to obey a -3 law. Spectra were computed for daily SST, three-week mean fields and daily perturbations from these means. A plot of $kE_1(k)$ vs. the logarithm of wavenumber k reveals a spectral peak at wavelengths of 16-40 km. We conclude that a large amount of the variance of the SST is concentrated in the mesoscale eddies which are being advected through the upwelling region. This result also means that passive, neutrally-buoyant, particulate matter would be expected to exhibit patchiness on the scale of 16-40 km. Therefore, in addition to SST, phytoplankton and other buoyant material are expected to be concentrated in advected mesoscale eddies of 16-40 km in horizontal extent on the continental shelf.

2. DATA ACQUISITION AND REDUCTION

During the summer of 1973, a large quantity of sea surface temperature data was gathered daily as part of the Coho Salmon Prediction Project. This project was undertaken in order to study the feasibility of applying remote sensing techniques to the gathering of mesoscale sea surface temperature data off the central Oregon coast. The collection and analysis of this data was a necessary input for providing daily forecasts of environmental factors influencing the location of harvestable Coho Salmon in Oregon coastal waters. Coho Salmon have been observed to prefer a temperature range estimated to be between 11.0C and 13.0C (D. Richey, 1971). One of the significant products of this project was thirty-five synoptically-analyzed sea surface temperature maps. The successful SST mapping flights which led to the production of these daily maps were made on thirty-five days during the 62-day period of the project. On the other twenty-seven days flights could not be made due either to an impenetrable ceiling along the coastal mountain range or to inshore fog near the coast. Most of the mapping flights were made during the early afternoon hours (between 1100 and 1400 PST). Table I contains the COHO flight summary. This collection of analyzed data represents the largest accumulation of almost-daily SST data in a coastal upwelling region or other oceanic region to date. (For a more in-depth study of the COHO Project, the reader is referred to the following publications:

region or other oceanic region to date. (For a more in-depth study of the COHO Project, the reader is referred to the following publications:

Table 1. COHO Flight Summary

Flight No.	Date	Location and Time Flight Commenced	Location and Time Flight Terminated	Winds During Flight (Newport) m sec^{-1}		Weather Conditions
1	15 June	LC 1350 PST	NPT 1600 PST	SW	2	Rain Showers
2	18 June	LC 1425 PST	NPT 1640 PST	W	3	Clear
3	20 June	LC 1230 PST	YAC 1455 PST	NNW	9	Clear
4	21 June	LC 1130 PST	NPT 1345 PST	NNW	6	Clear
5	27 June	LC 1350 PST	NPT 1640 PST	NNW	10	Partly Cloudy
6	28 June	LC 1055 PST	NPT 1315 PST	NNW	9	Clear
7	29 June	LC 1040 PST	NPT 1300 PST	NNW	5	Cloudy
8	30 June	LC 1150 PST	DB 1455 PST	NNW	5	Clear
9	1 July	LC 1030 PST	NPT 1240 PST	NNW	6	Clear
10	2 July	LC 1050 PST	DB 1250 PST	WSW	3	Clear
11	3 July	LC 1100 PST	DB 1315 PST	WNW	2	Patchy Fog
12	5 July	LC 1100 PST	DB 1300 PST	NW	4	Partly Cloudy
13	6 July	LC 1130 PST	DB 1330 PST	SSW	5	Rain Showers
14	7 July	LC 1045 PST	DB 1320 PST	WSW	2	Clear
15	9 July	LC 1025 PST	DB 1250 PST	W-NNW	3	Clear
16	11 July	LC 1050 PST	DB 1310 PST	NNW	9	Clear
17	12 July	NPT 1050 PST	LC 1210 PST	NNW	12	Patchy Fog
18	14 July	LC 1020 PST	NPT 1220 PST	NNW	7	Clear
19	15 July	LC 1120 PST	DB 1330 PST	NW	6	Haze
20	16 July	LC 1040 PST	DB 1240 PST	W-WSW	3	Patchy Fog
21	19 July	NPT 1200 PST	DB 1450 PST	WSW	3	Cloudy
20	16 July	LC 1040 PST	DB 1240 PST	W-WSW	3	Patchy Fog
21	19 July	NPT 1200 PST	DB 1450 PST	WSW	3	Cloudy

Location Codes: DB denotes Depoe Bay
LC denotes Lincoln City
NPT denotes Newport
YAC denotes Yachats

Table 1. COHO Flight Summary, continued

Flight No.	Date	Location and Time Flight Commenced	Location and Time Flight Terminated	Winds During Flight (Newport) m sec^{-1}		Weather Conditions
22	22 July	LC 1230 PST	DB 1420 PST	WNW	3	Clear
23	23 July	LC 1130 PST	DB 1340 PST	NNW	3	Clear
24	24 July	LC 1015 PST	DB 1230 PST	NNW	5	Haze
25	25 July	NPT 0945 PST	LC 1345 PST	NNW	7	Clear
26	27 July	DB 1036 PST	LC 1415 PST	NNW	6	Clear
27	31 July	LC 0455 PST	DB 0815 PST	N-NNE	5	Clear
28	3 Aug	NPT 1100 PST	DB 1300 PST	NNW	6	Partly Cloudy
29	4 Aug	DB 1100 PST	LC 1330 PST	NNW	5	Patchy Fog
30	5 Aug	LC 1040 PST	DB 1415 PST	NNW	4	Partly Cloudy
31	7 Aug	LC 1225 PST	DB 1500 PST	W	2	Partly Cloudy
32	9 Aug	LC 1150 PST	NPT 1400 PST	WNW	3	Rain Showers
33	10 Aug	LC 1023 PST	DB 1230 PST	NNW	6	Partly Cloudy
34	14 Aug	LC 1015 PST	DB 1300 PST	NNW	10	Cloudy
35	15 Aug	LC 1050 PST	NPT 1230 PST	NNW	6	Partly Cloudy

Location Codes: DB denotes Depoe Bay
LC denotes Lincoln City
NPT denotes Newport

The COHO Project: Living Resources Prediction Feasibility Study, Vols. I, II, III).

During the COHO Project, daily SST mapping flights were made in a high-winged, single engine aircraft equipped with a remote precision radiometer. The radiometer used was a narrow band, 10-12 micron, Barnes Engineering Co. Precision Filter Radiometer, model PRT-6. This radiometer was chosen since it was the best radiometer available for use which could minimize effects of water vapor absorption in the air column between it and the sea surface. The best radiometer we could have used for this particular study would have been one which was sensitive in the 9-11 micron wavelength band since both atmospheric and water vapor attenuation of radiant energy is very small in this band. Fig. 1 shows the attenuation and emission by atmospheric gases between the surface and an airborne sensor (after Saunders and Wilkens, 1966). In this figure the atmosphere is assumed isothermal and 10C different in temperature from the underlying water. COHO Project mapping flights were usually made at the 150 m (500 ft.) level over water which was different in temperature from the atmosphere by 5C or less. The mixing ratio in the COHO flight area varied from 5 gkg^{-1} to 10 gkg^{-1} during different flight days. From the figure we estimate that the maximum error in our measurements of the SST due to atmospheric and water vapor attenuation and emission is less than 0.4C. Our PRT-6 calibration procedure, which will be discussed next, was designed to minimize this error and other errors which could arise during the data collection process.
cussed next, was designed to minimize this error and other errors which could arise during the data collection process.

The success of the daily SST mapping operation depended critically on the calibration of the PRT-6. This calibration was required to relate

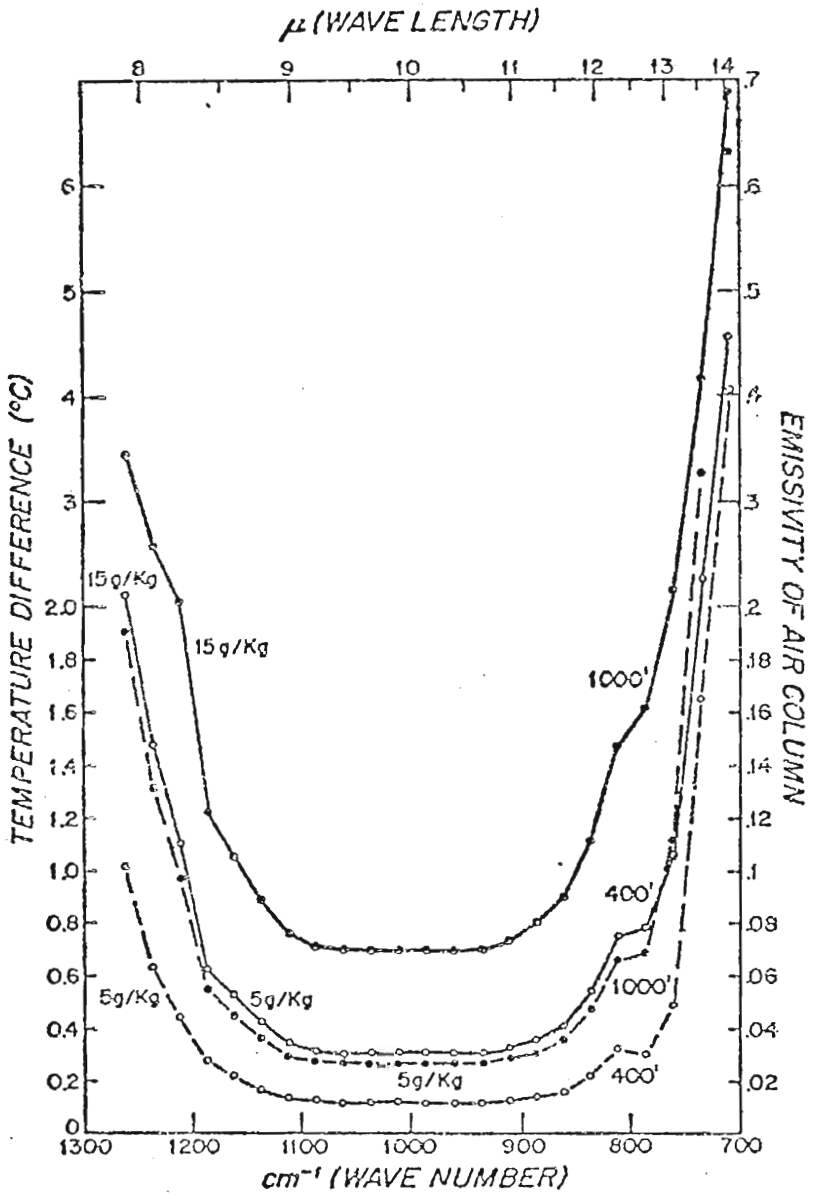

Fig. 1. Attenuation and emission by atmospheric gases between the surface and an airborne sensor: the atmosphere is assumed isothermal and 10C different in temperature from the underlying water. (From Saunders

Fig. 1. Attenuation and emission by atmospheric gases between the surface and an airborne sensor: the atmosphere is assumed isothermal and 10C different in temperature from the underlying water. (From Saunders and Wilkens, 1966).

accurately the PRT-6 voltage output to the recorded sea surface temperature. Twice-daily field calibrations of the PRT-6 were made. The preflight calibration took into account any day-to-day fluctuations of the radiometer response while the post-flight calibration took into account any drift of the PRT-6 response during the flight. In order to supply the power for the PRT-6 which these calibrations needed, a ground power source was used at the Albany, Oregon, airport. Then, after allowing time for the instrument to warm up, a bucket of water cooled to about 7.0C was placed directly under the downward-looking PRT-6 and the temperature was recorded on the PRT-6 strip chart recorder. The water in the bucket was then warmed up in approximately two-degree increments with the corresponding temperature recorded on the strip recorder. This information recorded on the strip chart recorder could then be used to make a daily operational temperature scale for the SST data which would be gathered in flight. The post-flight calibration was achieved by the same process as that outlined above. Any in-flight drift in PRT-6 response was then noted and taken into account when plotting the data on maps.

An indispensable piece of equipment was a 23-channel, citizen's band (CB) radio which allowed the aircraft data taker to communicate with fishermen from the aircraft. The use of the CB radio aided in the calibration process. A check could then be made almost instantaneously between the temperature recorded by the strip chart recorder in the aircraft and the bucket temperature taken by a fishing boat almost directly under the radiometer. These checks proved invaluable in providing a confidence level for the data and were especially useful in helping to

minimize the effects of the atmosphere and water vapor in the air column between the aircraft and the sea surface. Two other methods of minimizing these effects were occasionally employed (Saunders, 1970; O'Brien, 1972; and Thompson, 1973). The air column length between the aircraft and the sea surface could be doubled by banking the aircraft 60°. An indication of these effects could be calculated by noting changes in PRT-6 sea surface temperatures measured during this aircraft banking process. This method was only useful if the mapping aircraft was flying over a region of small SST gradients. Flying over the same water twice at different altitudes (150 m and 200 m) was the other method employed. Again, a change in PRT-6 output could be noted and air column effects could be accounted for. In addition to the in-flight checks made through the use of the radio, ground "sea truths" were obtained from fishermen in or near the flight paths during the flight. These temperatures were used as an additional verification of the validity of the SST data. Precision in measuring SST during this project was on the order of .25C. During the flight the data taker recorded ocean fronts, birds, fishing boat concentrations, navigational reference point, times, and other pertinent observations on the strip chart recorder or in the log book.

A typical flight plan in shown in Fig. 2. (The daily flight plans are shown on the SST maps in the publication, The COHO Project, Vol. II). The sea surface temperatures were mapped from an average in-flight altitude of 150 m. The mapping aircraft usually maintained a speed of about 190 km per hour. In order to aid navigation over the ocean, the aircraft was equipped with an omnidirectional navigation receiver (VOR) with a distance measuring feature (DME). The flight plan was developed

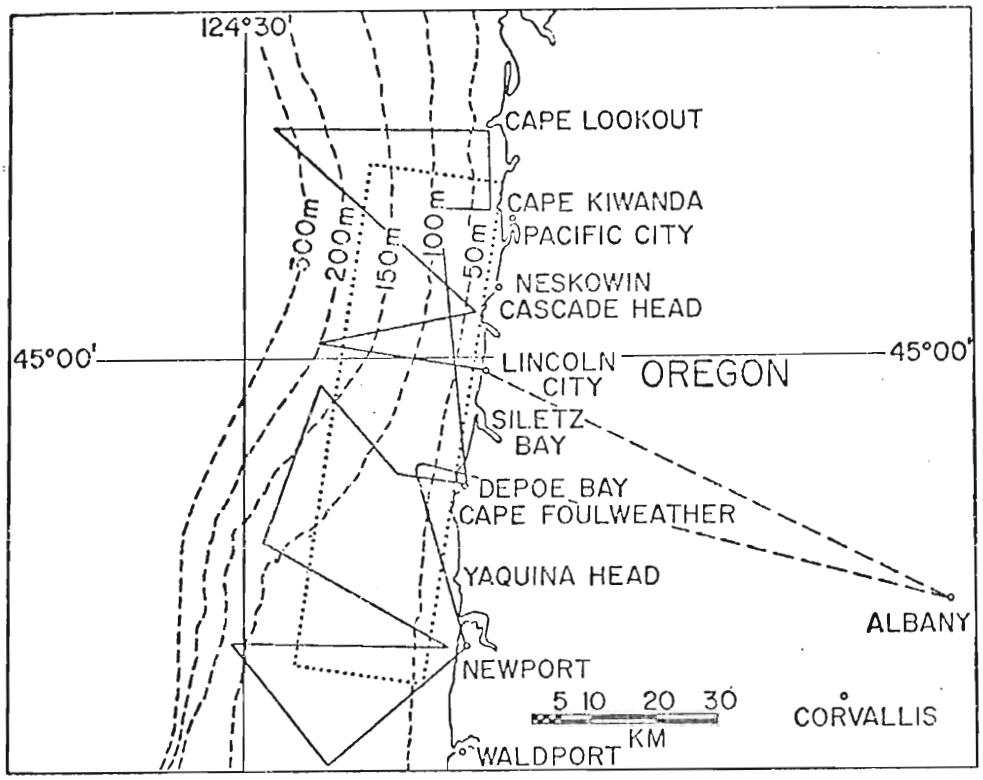

Fig. 2. Map of central Oregon coast showing a typical COHO aircraft flight pattern and pertinent bays, capes and towns. Dashed lines labelled in meters are isobaths. The dotted rectangle represents the rotated rectangular grid which contained the SST values from which the spectra in section 5 are computed.

towns. Dashed lines labelled in meters are isobaths. The dotted rectangle represents the rotated rectangular grid which contained the SST values from which the spectra in section 5 are computed.

to take advantage of the aircraft navigational aids in the central Oregon coastal area (Newport VOR). The use of these aids minimized the influence of wind conditions on aircraft position and also allowed fairly accurate flight paths to be determined.

After the daily mapping flights were completed, the SST data were plotted on a map. Values of SST in tenths of a degree Fahrenheit were plotted on the map along the actual flight paths. These plotted values were then synoptically analyzed at 1F increments. This analysis was subsequently used to make the COHO environmental forecast. Later, a more careful synoptic analysis of this data was made and published in The COHO Project, Vol. II.

The finalizing of these analyses concluded the first phase of the data acquisition and reduction process of this mesoscale SST data. The SST from the daily maps were digitized for every 1 km within the inshore 20 km and for every 2 km offshore of 20 km. The offshore 2 km grid was reduced to a 1 km grid scale by bilinear interpolation. Computer-contoured maps were used to check the accuracy of the digitized data. A very thorough quality control process was used in order to insure that accurate temperature values had been digitized and keypunched from the synoptically-analyzed maps. The SST values on the original maps were recorded in degrees F as an aid to fishermen; computer analyzed values were converted to degrees C. The remainder of this paper deals with the scientific interpretation of this digitized data.

In order to analyze the effect of the wind field on the SST field, scientific interpretation of this digitized data.

In order to analyze the effect of the wind field on the SST field, the wind data gathered from the anemometer located at the Newport south jetty were processed. Winds measured by this Bendix-Freize anemometer

were recorded continuously on a strip chart. The values transcribed from the strip chart were 20-minute averages centered at each hour. These hourly values were vector-averaged over a 24-hour period to obtain the daily average which is referred to in this study. Our SST data were gathered no more than once daily and at various times during the day. Therefore, we chose to use the 24-hour-averaged winds at Newport, Oregon.

3. FEATURES OF THE MESOSCALE SEA SURFACE TEMPERATURE FIELD

In this section we will investigate the response of the SST field to wind forcing, and horizontal sea surface temperature gradients and their attendant oceanic fronts. Also to be presented in this section is a case study of the daily temperature differences during an upwelling event.

Fig. 2 of the previous section, in addition to showing a typical flight plan, displays the pertinent bays, capes, and towns which will be referred to later in this paper. Fig. 3 gives an indication of the response of the SST field to wind forcing. Fig. 3a shows a time series of the daily averaged Newport winds and SST at 5, 10, and 15 km off Cascade Head, Oregon, during the period 15 June to 15 August. Newport winds are denoted by wind barbs showing wind speed in knots.

SST normally increase in the offshore direction within 30 km of the coast. SST are generally cooler when northerlies are blowing and warmer when southerlies are blowing as shown by Fig. 3a. SST 5 km off-shore of Cascade Head range from a low of 7.4C on 14 July to a high of 15.2C on 7 July. The most rapid cooling occurred during the days 9-12 July, a period of strong northerly winds. Winds were gusting to 19 m sec^{-1} from the NNW on 12 July. During this period SST 5 km off-shore of Cascade Head dropped from 14.5C to 8.5C. Recall that the annual range is only 3C (from monthly averages). An anomalous warming is shown during

cade Head dropped from 14.5C to 8.5C. Recall that the annual range is only 3C (from monthly averages). An anomalous warming is shown during

a period 4-7 August when northerlies were blowing. An investigation of

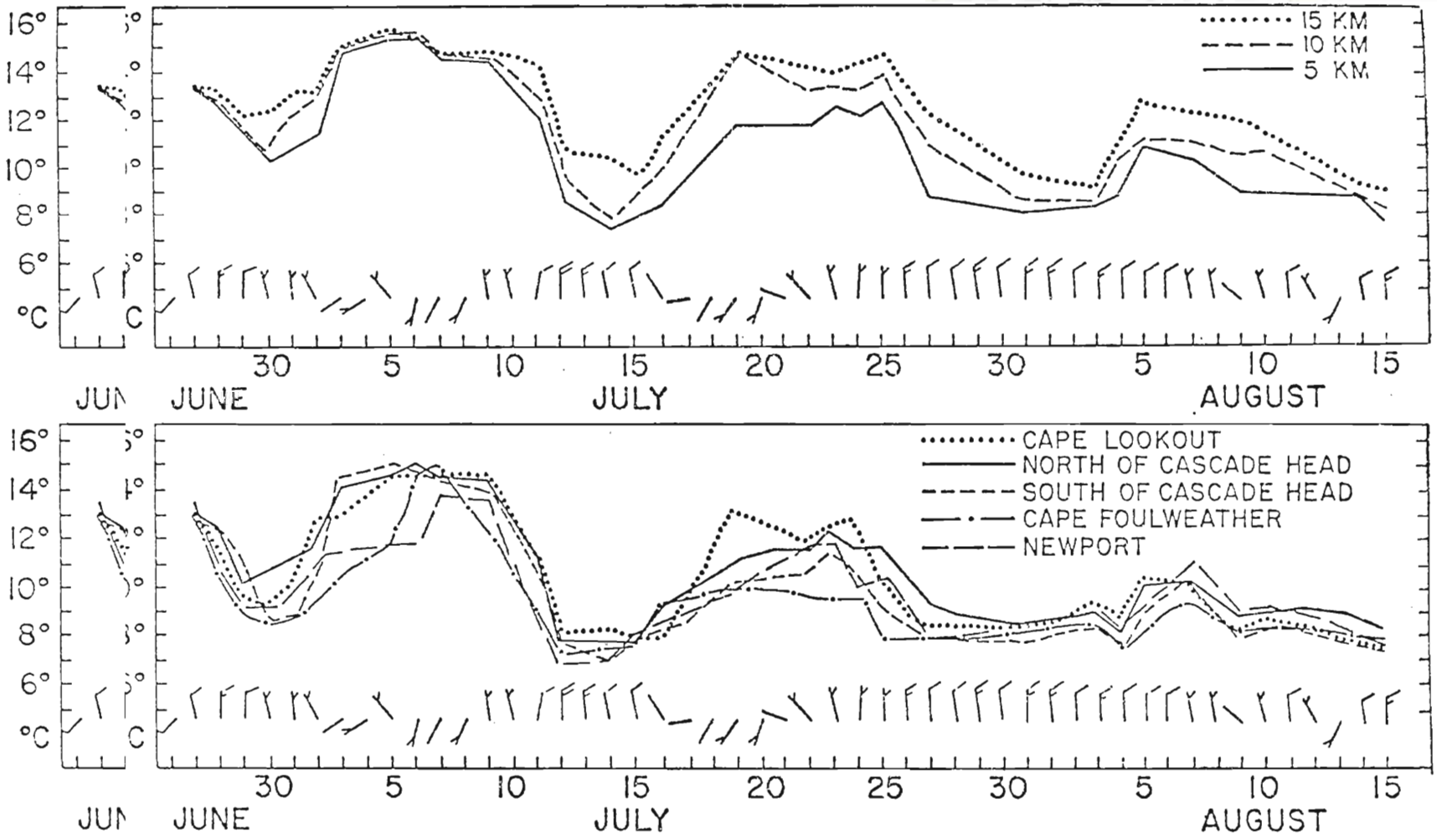

Fig. 3. (a) SST and daily averaged Newport winds vs. time at 5,10, and 15 km off Cascade Head, OHead, Oregon, during 15 June-15 August, 1973. (b) SST and Newport winds along 40 m isobath off selecteselected points along Oregon coast during 15 June-15 August, 1973.

the horizontal SST maps for these days reveals that warm water was being advected through the flight region from the NW.

Fig. 3b shows a time series of the daily averaged Newport winds and SST along the 40 m isobath offshore of selected points along the Oregon coast during the period 15 June to 15 August. As shown by Fig. 2 Cape Lookout is the northernmost coastal point in the flight region while Newport is one of the southernmost points. The 40 m isobath is within 5 km of shore. Again we note that SST are generally cooler when northerlies are blowing and warmer during periods of southerlies.

SST from Newport to Cape Lookout may vary as much as 3.5C and as little as 1.0C along the 40 m isobath. As was true in the previous figure, the most rapid cooling along the 40 m isobath occurs during the period 9 to 12 July. The anomalous warming which was noted in Fig. 3a can also be noticed in Fig. 3b. We can note from Fig. 3 that during several periods the SST reached about the same minimum value. In the summer of 1973 this minimum value corresponded to about the coldest water found on the bottom of the ocean on the continental shelf (Huyer, 1974).

An inspection of the daily horizontal SST maps reveals the large variability of the entire mesoscale temperature field from day to day. Sixteen of these horizontal SST maps corresponding to the period 27 June to 16 July are contained in Appendix A. During a period of northerly winds the warmest temperatures shoreward of the shelf edge may become cooler than the coldest temperature observed in this region prior to

cooler than the coldest temperature observed in this region prior to

the period as shown by examining Fig. A-11a and Fig. A-14a.

An investigation of the horizontal SST maps also reveals the existence of areas of strong horizontal SST gradients called "oceanic fronts." These oceanic fronts represent a zero order discontinuity in sea surface temperature. Surface convergence may exist in the vicinity of the oceanic front and may be found to be quite strong with long foam lines and color fronts tending to align themselves NE-SW along the coast. These frontal areas were often easily visible from the mapping aircraft. Figs. A-15a and A-16a are horizontal SST maps which display regions of strong temperature gradients. These maps show horizontal SST for the days 15 and 16 July, respectively. Northerly winds had been blowing since 9 July. One of the oceanic fronts is located off Cape Lookout between the 100 and 150 m isobaths on 15 July. By 16 July the front has moved inshore of the 100 m bathymetry curve. Actually, the gradients shown in Fig. A-15a and Fig. A-16a are even stronger than they appear in these maps. The gradients shown in the figures really may exist on the scales of several hundred meters to 1 km instead of several kilometers as noted by the data-taker when he was gathering the SST data during the COHO Project.

Results of a study of a series of detailed BT transects of an upwelling frontal system west of Cape Town (18°E, 36°S) during a February, 1968, upwelling event were presented by Bang (1973). Conspicuous changes in the SST field were noted within hours of wind shifts from Southern Hemispheric upwelling producing southerlies to northerlies and conversely. At the end of a period of southerlies, SST changes across an intense

Hemispheric upwelling producing southerlies to northerlies and conversely. At the end of a period of southerlies, SST changes across an intense

frontal structure which was approximately 5 km were 11C. A widening of this zone to 15 km occurred after a day of strong northwesterly winds.

Also, Bang reported that occasionally SST could be seen to change by several degrees within several hundred meters. In Thompson's (1974) model, which included thermodynamic effects, rapid lowering of SST during upwelling-event-characteristic wind forcing resulted in the formation of a strong horizontal temperature gradient or frontal region near shore.

The final topic to be presented in this section is a case study of the daily horizontal SST differences during the period 7 to 16 July. Because mapping flights were not made on 8, 10, and 13 July, Figs. 5a, 5b, and 6b represent SST differences for two days. This period of ten days ended with eight days of northerlies. Winds on 7 and 8 July were light southerlies. The strongest winds during the entire 62-day project blew from the north on 11 and 12 July. During the afternoon hours on 11 July winds blew steadily from the NNW at 8-10 m sec^{-1} with gusts to 15 m sec^{-1} while on 12 July winds blew steadily from the NNW at 14-16 m sec^{-1} with gusts to 20 m sec^{-1}. Horizontal SST for 7 July are shown in Fig. 4a. SST range from greater than 15C along the coast northward from Depoe Bay to Cape Lookout to less than 13C alongshore south of Depoe Bay to Newport. Fig. 4b shows the horizontal SST for 16 July at the end of the case study period. SST are less than 9C all alongshore and are not greater than 13C until we go offshore of the 150 m isobath in most of the region.

Fig. 5a shows the differences in SST between 7 and 9 July. Winds started to blow strongly from the NNW during the mapping flight on 9 July. Previously they had either been from a southerly direction or light from the NE. Consequently, little cooling in the flight region

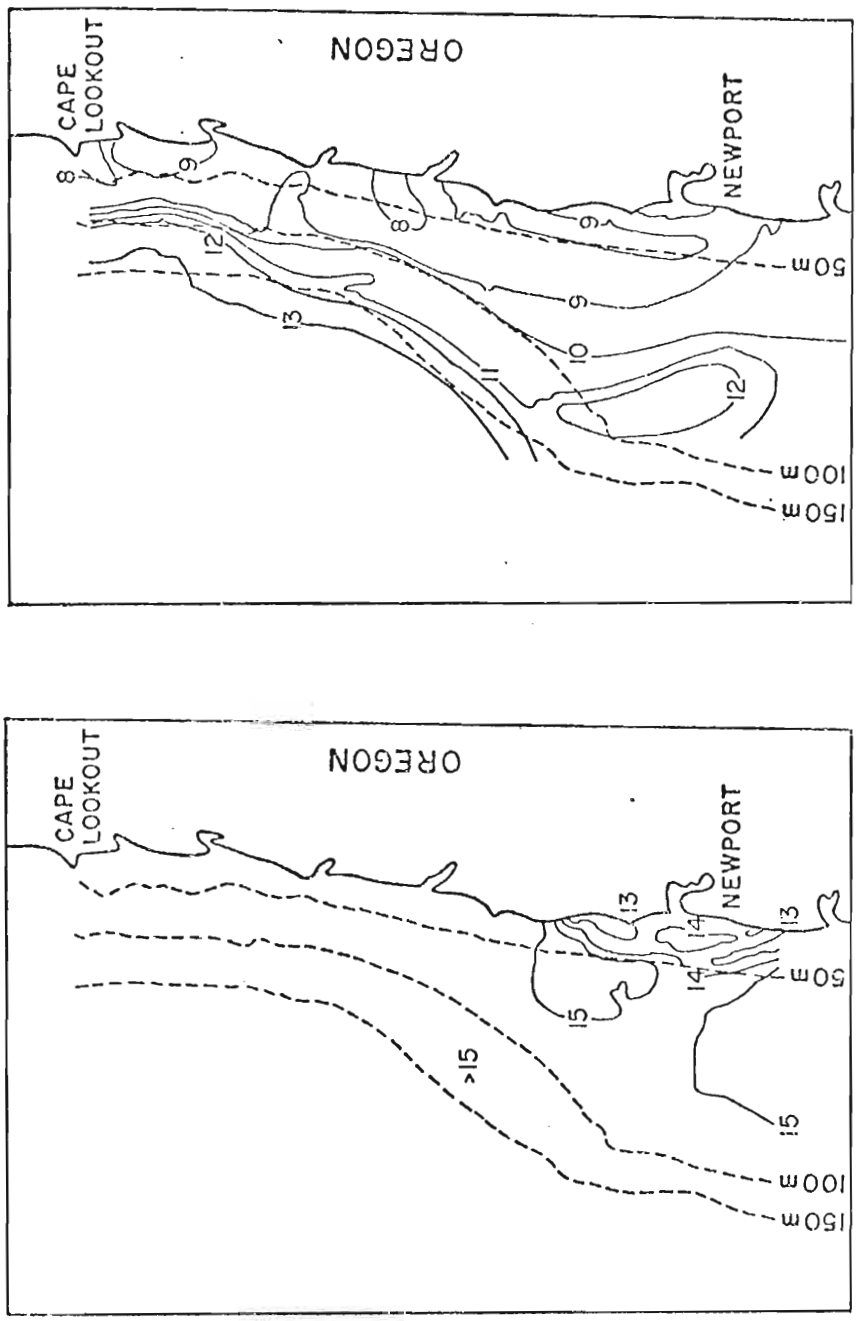

Fig. 4. Horizontal sea surface temperatures in the COHO flight region for (a) July, 1973, and (b) 16 July, 1973. Dashed lines labelled 50 m, 100 m, 150 m are isobaths.

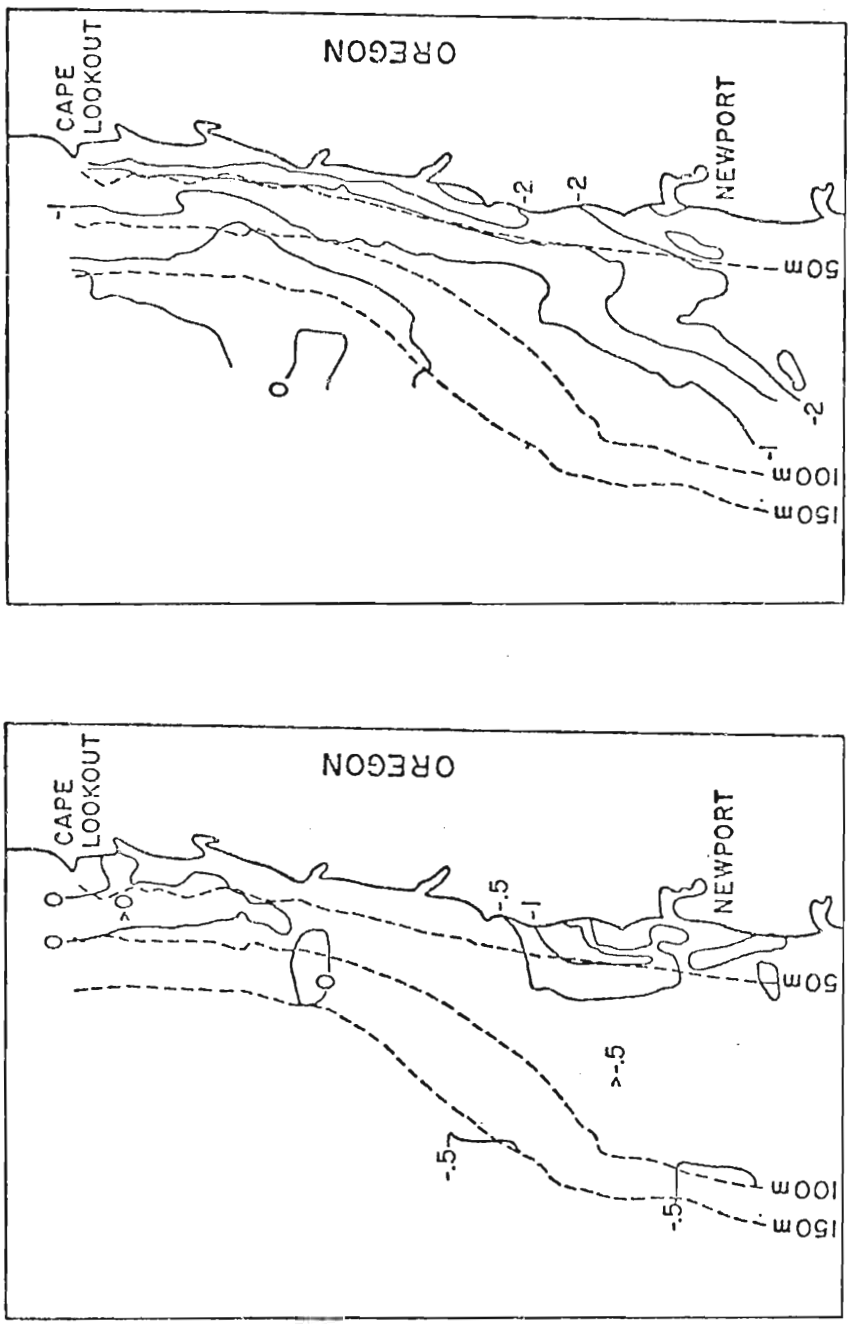

Fig. 5. Differences in sea surface temperatures in the COHO flight region between (a) 7 and 9 July, 1973, and (b) 9 and 11 July, 1973. Dashed lines represent isobaths.

had occurred. With continued northerly winds SST began to cool more rapidly. SST cooled from 1.5C to greater than 2.0C inshore of the 50 m isobath during the two-day period 9 to 11 July. This cooling is shown in Fig. 5b. Because of strong northerlies on 11 and 12 July, SST cooled most rapidly between 11 and 12 July. Examination of Fig. 6a shows that SST cooled as much as 3.0C to 4.5C in the offshore area between the 50 m and 100 m isobaths. In Thompson's (1974) model the water temperature cooled 5C in less than one day very near the coast. Fig. 6b, which shows the difference in SST between 12 and 14 July, reveals that SST changed very little over the region (.5C or less) except offshore from Cape Lookout. In a region 15-30 km offshore from Cape Lookout SST decreased by .5C to 1.5C. The small change in SST occurred while northerlies were blowing. As was stated earlier in this section, SST can only become as cold as the deep shelf water being upwelled. SST on 14 July were very cold. By looking at Fig. A-14a which shows horizontal SST for 14 July, we can see that SST range from less than 7C just south of Cascade Head to 12C 30 km offshore of Yaquina Head.

A glance at Fig. 7a shows that an intense warming happened offshore of the 100 m isobath in the Cape Lookout area between 14 and 15 July. SST warmed as much as 5C offshore of the 150 m isobath in this area. SST within 5 km of the coast warmed slightly (less than 1C). The final map in this series, Fig. 7b, shows the differences in SST between 15 and 16 July. Note that warming has occurred 20-30 km offshore from Newport. Warming has also occurred in the inshore 5 km south of Cape Lookout to Pacific City and also between the 100 to 150 m isobath in

Newport. Warming has also occurred in the inshore 5 km south of Cape Lookout to Pacific City and also between the 100 to 150 m isobath in

this area and in a band approximately 5 km wide oriented SSW from Siletz

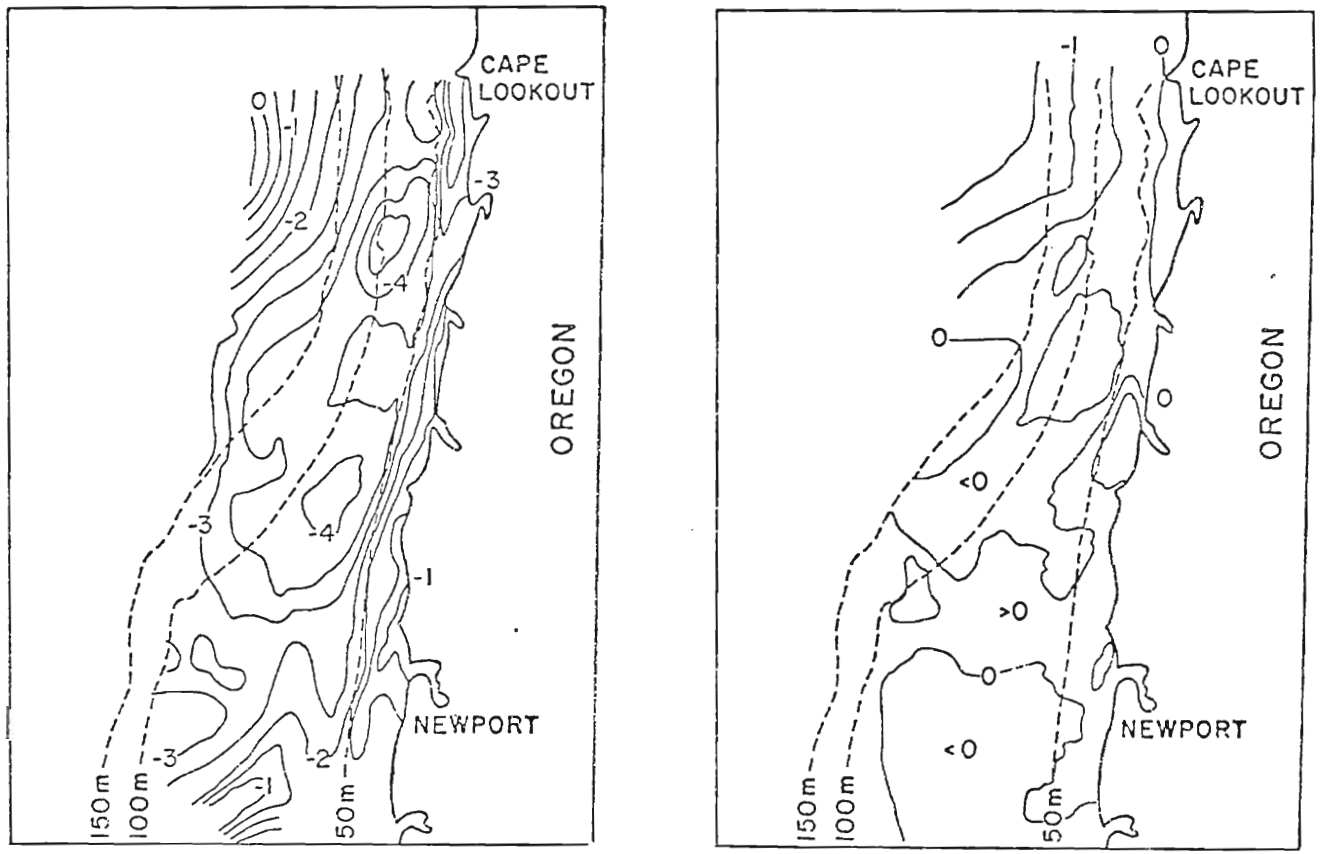

Fig. 6. Differences in sea surface temperatures in the COHO flight region between (a) 11 and 12 July, 1973, and (b) 12 and 14 July, 1973.

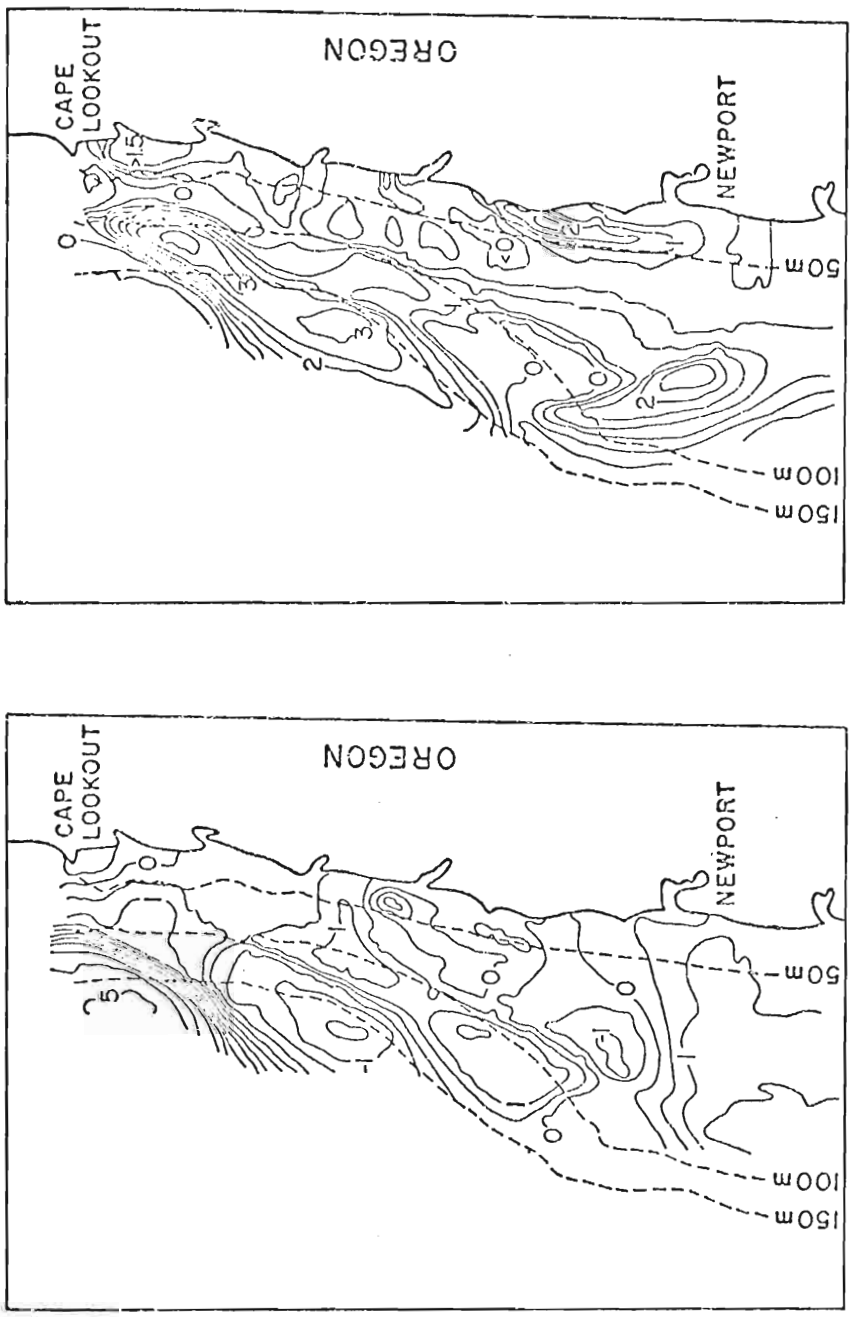

Fig. 7. Differences in sea surface temperatures in the COHO flight region between (a) 14 and 15 July, 1973, and (b) 15 and 16 July, 1973.

Bay to Newport along the 50 m isobath.

We conclude this section by stating that wind forcing seems to dominate the SST field. Very low SST can occur during periods of strong northerlies. Upwelling caused by these northerly winds accounts for the lower SST occurring during these periods. By looking at a time series of the SST offshore from selected points, horizontal SST maps and maps of daily SST differences, we have seen that the mesoscale SST field is highly variable from day to day and from point to point. Another aspect of the variability of the mesoscale SST field will be presented in the next section when we look at the mean fields and the daily perturbations from these means.

4. MEANS AND PERTURBATIONS

In this section a discussion of two three-week mean fields and daily perturbations from these means will be presented. Mean fields were computed for the periods 27 June to 16 July (20 days) and 22 July to 10 August (19 days). These two periods were chosen because there was different wind forcing during each period. During the first period two "upwelling events" occurred. Recall that during these events winds are generally from the N and NW. These events were separated by several days of southerly winds. Northerlies blew continuously throughout the second period. Since fog prevented mapping flights several times for several days in succession, the location of these gaps in the almost-daily array of SST maps dictated the choice of the averaging periods. Twenty-eight perturbation maps were computed. In order to compute these perturbation maps, the mean temperature at every point on the map was subtracted from the daily temperature at every point. Perturbation maps for the period 27 June - 16 July are contained in Appendix A.

The mean temperatures in the mapping region during the first averaging period 27 June - 16 July ranged from less than 10C near shore to 13C offshore as shown in Fig. 8. Fig. 9 shows that mean SST are less than 9C in a small area near shore just south of Cascade Head and again just south of Depoe Bay during the second averaging period. From analyzing Fig. 9 we can see that mean SST in the COHO flight region are less during the second averaging period. This is probably due to the fact

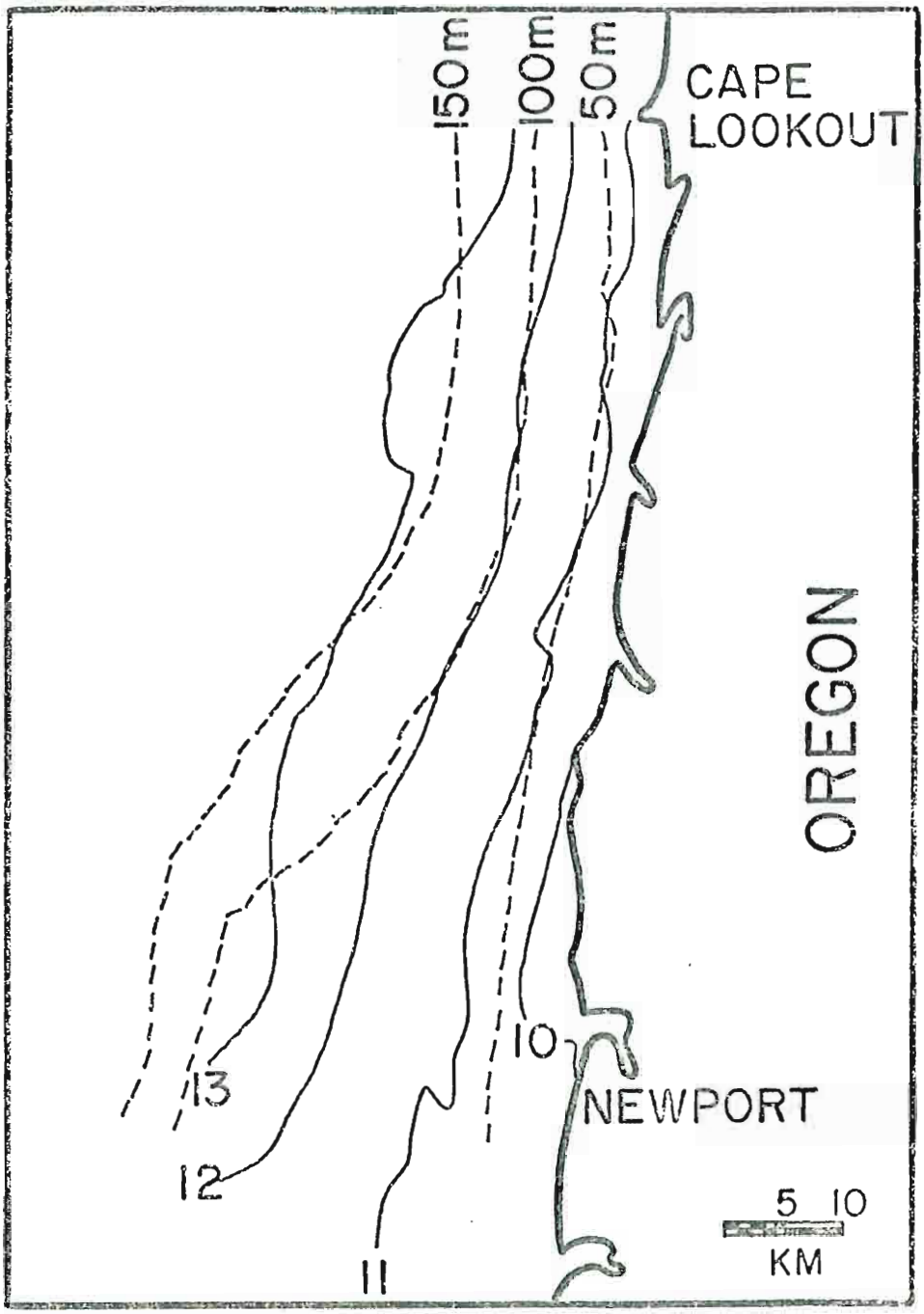

Fig. 8. Mean isotherms in COHO flight region during the twenty-day period 27 June, 1973, to 16 July, 1973. 50 m, 100 m, 150 m isobaths are also shown.

Fig. 8. Mean isotherms in COHO flight region during the twenty-day period 27 June, 1973, to 16 July, 1973. 50 m, 100 m, 150 m isobaths are also shown.

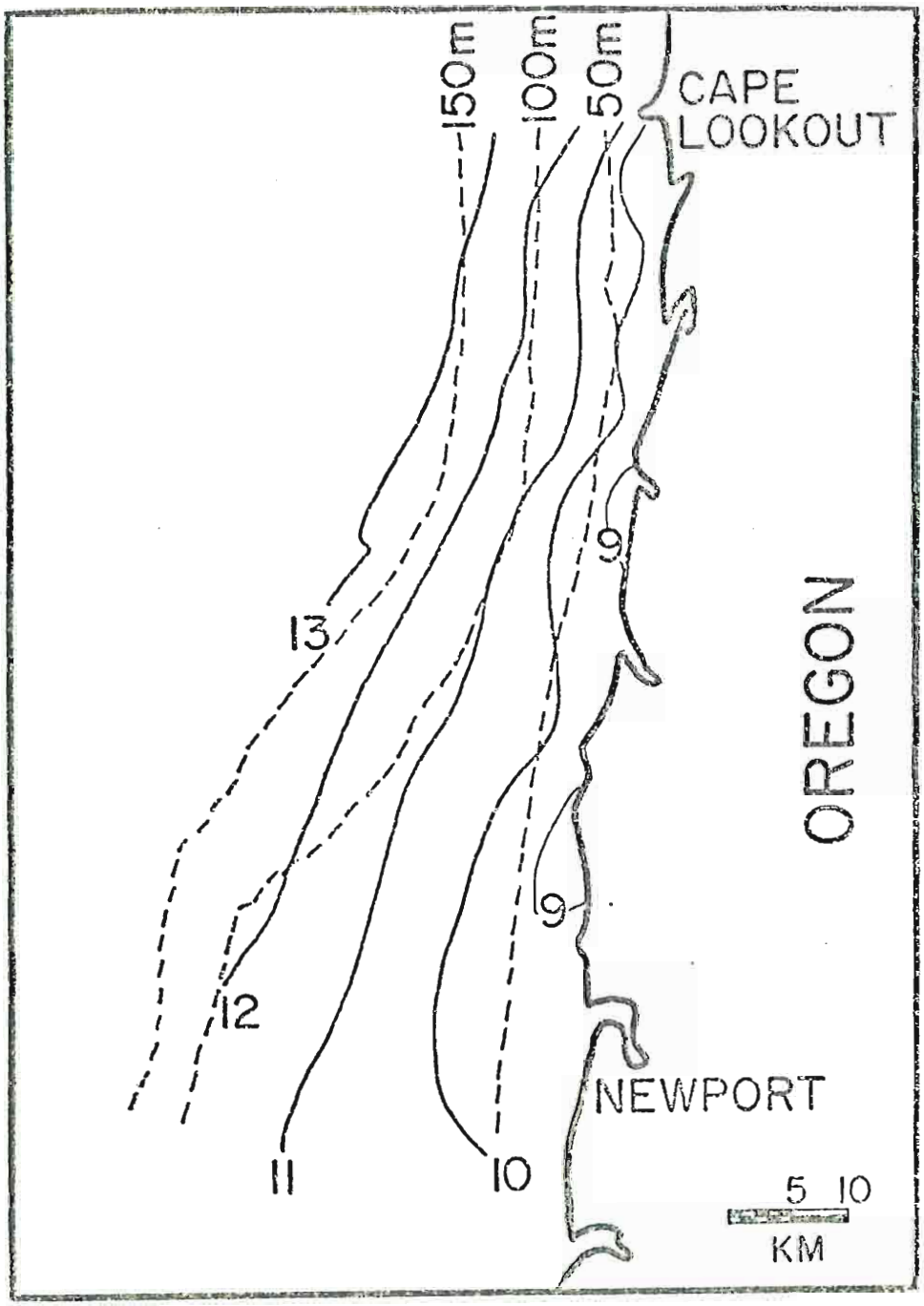

Fig. 9. Mean isotherms in COHO flight region during the nineteen-day period 22 July, 1973, to 10 August, 1973. 50 m, 100 m, 150 m isobaths are also shown.

Fig. 9. Mean isotherms in COHO flight region during the nineteen-day period 22 July, 1973, to 10 August, 1973. 50 m, 100 m, 150 m isobaths are also shown.

that the winds were consistently from the north during this period. Another aspect of the mean fields for these two periods is that the mean isotherms tend to follow the large scale bathymetry.

If we glance through Figs. A-1b to A-16b, the perturbation maps for the days 27 June - 16 July, we notice the large number of eddies which appear on these maps. Also, by looking at the perturbation maps (see Figs. A-14b, A-15b, A-16b) the existence and location of oceanic fronts may be determined. Daily perturbations of $\pm$ 3C from the three-week mean are prevalent inshore of the 100 m isobath. Fig. 10a shows the horizontal SST field for 5 August, a day when a large range in SST existed. On this day SST ranged from 8.5C inshore to 16C offshore. The corresponding daily perturbation map is shown in Fig. 10b. There is a large variability in the transient SST field as shown by this map. The winds throughout the second averaging period which includes 5 August were consistently from a northerly direction as stated earlier.

The tracing of individual eddies on these maps from day to day is made difficult because of the strong horizontal flow and the strong shear in the longshore current in the mapping region. Fig. 11 taken from Garvine (1974) shows surface drogue positions off the coast of Oregon on 24 August, 1972. These surface drogues were deployed to measure the strength and shear of the surface current under the northerly wind. Winds had been northerly beginning the afternoon of 22 August. After about twenty hours of motion two major characteristics of the flow are noted. These are the orderliness of motion and the strong shear in the

noted. These are the orderliness of motion and the strong shear in the

longshore current. The shearing action is strongest in the center of the drogue array, from drogues #32 to #27. The offshore drogues (#33 to #39)

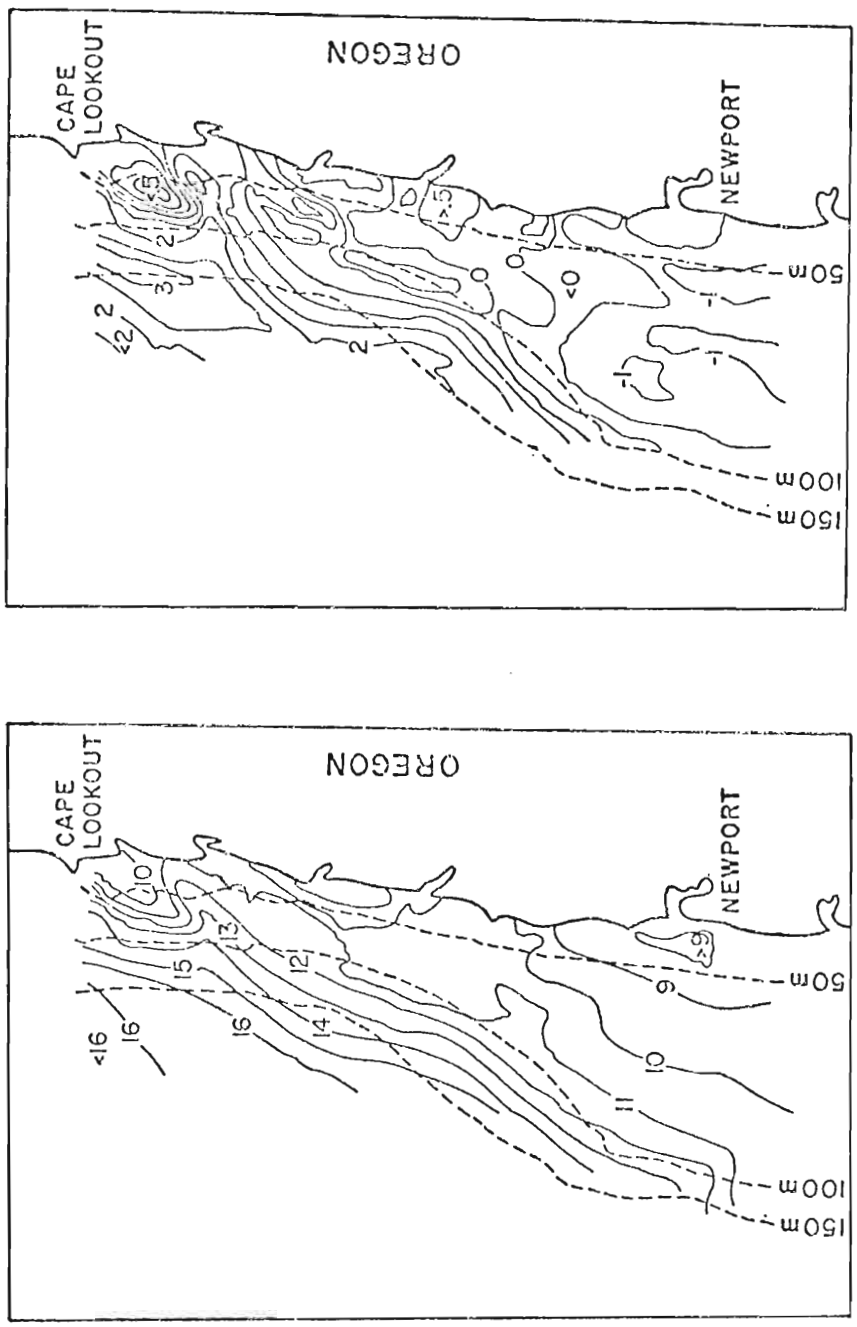

Fig. 10. (a) Horizontal sea surface temperatures in the COHO flight region for 5 August, 1973, (b) perturbations from the three-week mean in the COHO flight region for 5 August, 1973. Dashed lines represent isobaths.

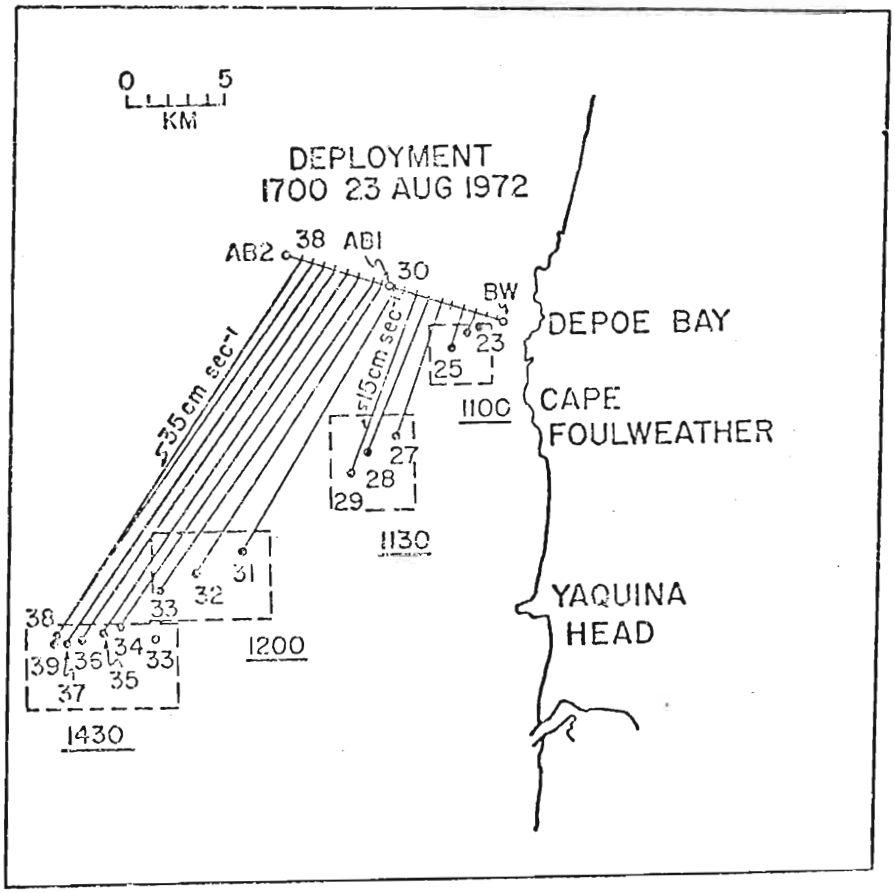

Fig. 11. Surface drogue positions off the coast of Oregon on 24 August, 1972. These drogues were numbered from 22 to 39. (Garvine, 1974)

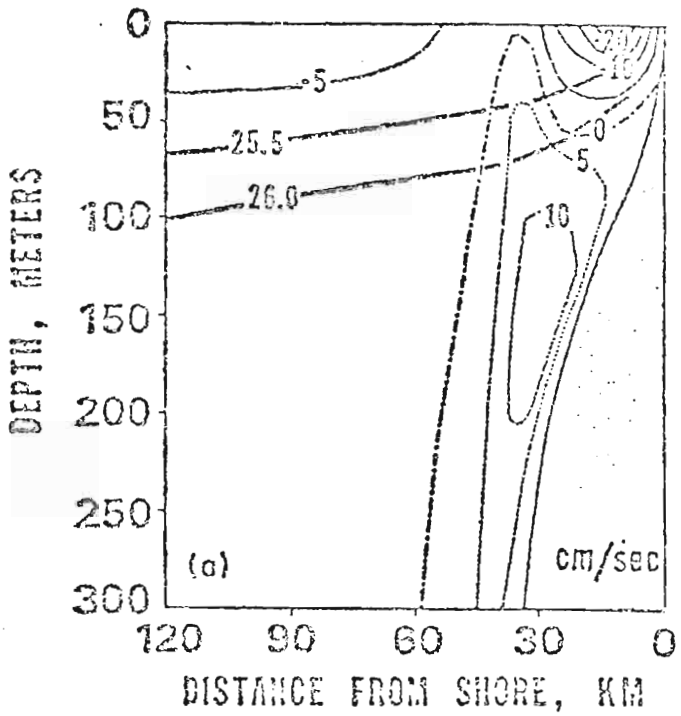

Fig. 12. Diagram of the absolute geostrophic longshore flow (two-week average) off Depoe Bay during August, 1966 (From Mooers, et al., 1973).

moved at an average speed of 35 cm sec^{-1} while the inshore drogues (#27 to #29) moved about 15 cm sec^{-1}. This motion seems to be in accord with the Ekman offshore/longshore transport that we would expect during periods of northerlies. Fig. 12 shows a two week average absolute geostrophic longshore flow off Depoe Bay, Oregon, in 1966. Note the strong equatorward surface jet (20 cm sec^{-1}) and the strong average shear in the longshore current. Smith (1974) and Huyer (1974) document the validity of geostrophy for the longshore flow in this mesoscale upwelling region off Oregon.

The mean field (not shown) for the entire 62-day period of COHO operation was calculated from thirty-five daily SST maps. There are large (3-5 days) gaps in data at the beginning and end of the operational period. The results are interesting, though. The coldest mean temperatures are located alongshore from Depoe Bay to Newport. This result is in agreement with the results of Hurlburt (1974). Hurlburt models the effects of a mesoscale canyon-like feature off the Oregon Coast on the wind-driven eastern ocean circulation. From his model he finds that upwelling is lessened on the north side of the canyon while being increased on the south side and near the coast on the axis of the depression.

In concluding this section, we have seen from the discussion and illustrations another aspect of the mesoscale variability of the SST. The final section will present a discussion of the results of a two-dimensional spectral analysis of this SST data.

5. SPECTRAL ANALYSIS

The spectral study of this mesoscale SST data was undertaken to investigate the scales of eddies in the horizontal temperature fields in an oceanic upwelling zone. Providing the motivation for this study were the results from a one-dimensional spectral analysis of mesoscale SST data presented by Saunders (1972). He computed spectra of SST gathered from the Mediterranean Sea by an infra-red radiation thermometer located in an aircraft. Over the range of scales 3-100 km, he found that the density of temperature variance seemed to obey a k^{-p} power law where k is the wavenumber and p is approximately 2.2. This power law, though, does not fit any proposed model of geophysical turbulence which he states in his paper. Another study of SST recorded from a remote sensing infra-red thermometer was presented by MacLeish (1970). The spectra computed from these SST have a maximum at the smallest wavenumber and then decrease rapidly as wavenumber increases; however, they do not decrease after a wavenumber greater than 2-5 cycle km^{-1}. Instead, in this high wavenumber range the spectral slope flattens with increasing wavenumber.

In the past several years much interest in the spectral distribution of intermediate to large-scale atmospheric motions has been generated. Observational studies by Horn and Bryson (1963), Winn-Nielsen (1967) and Julian, et al. (1970) indicated an approximate kinetic energy spectral slope of -3. These results did not fit Kolmogorov's (1941) -5/3 law
Julian, et al. (1970) indicated an approximate kinetic energy spectral slope of -3. These results did not fit Kolmogorov's (1941) -5/3 law
which he predicted for the inertial subrange of three-dimensional

isotropic turbulence. The motions of the atmosphere at mid-level had been considered approximately two-dimensional since Rossby et al. (1939). Kraichnan (1967) in response to this consideration proposed a k^{-3} behavior for the supposed approximately two-dimensional atmospheric motion. Charney (1971) proposed a theory which predicted a -3 dependence on wavenumber k of the spectra both of atmospheric kinetic energy and atmospheric temperature variance when the flow is three-dimensional and quasi-geostrophic. Lilly and Lester (1974) predicted that a horizontal spectrum of kinetic energy proportional to k^{-3} implies potential temperature spectra proportional to k^{-3}. These studies are for much larger scales than considered here.

Charney (1971) also reports that temperature spectra computed from an NCAR atmospheric prediction model made available to him by Wellck and Washington of NCAR revealed an approximate k^{-3} behavior. In a spectral analysis of atmospheric temperature, Kao (1970) found that in the high wavenumber range spectra generally decrease with increasing wavenumber and are proportional to k^{-3}. Lilly and Lester (1974) computed potential temperature spectra from stratospheric data gathered by an aircraft over Colorado in 1970. The spectral slopes in the 3-20 km range for potential temperature seemed to be approximately -3 in agreement with their theory. Charney also stated that his predicted k^{-3} behavior for the kinetic energy spectrum and temperature variance might apply to oceanic fields in regions of strong baroclinic excitation. Upwelling regimes are areas of strong baroclinicity.
oceanic fields in regions of strong baroclinic excitation. Upwelling regimes are areas of strong baroclinicity.

In our spectral study we computed spectra from a rectangular grid of SST data. This grid contained 1600 data points with data points

equally spaced 1 km apart. Spectra were computed for daily SST, three-week mean fields and daily perturbations from these means. This spectral analysis represents the largest undertaking of its kind in an oceanic region to date. Fig. 13a shows the rectangular grid which contained the SST values from which the spectra were computed. This figure shows that the x,y coordinates were rotated approximately 9° in the offshore direction. This was done so that the longshore sides of the rectangular grid of SST data points could be oriented parallel to the Oregon coastline in order to include as many of the nearshore points as possible while maximizing the size of the grid.

The sea surface temperature at each data point x,y can be written as a two-dimensional complex Fourier series expansion in the following form

$$T(x,y) = \sum_{j}\sum_{\ell} A_{j\ell} \exp\left(\frac{i2\pi jx}{L_x}\right) \exp\left(\frac{i2\pi \ell y}{L_y}\right) \qquad (1)$$

$$T(x,y) = \sum_{j}\sum_{\ell} A_{j\ell} \exp\left(i2\, k_{xj} x\right) \exp\left(i2\pi k_{y\ell} y\right) \qquad (2)$$

$$k_{xj} = \frac{j-1}{L_x} \qquad j = 1(1)\frac{N_x}{2}$$

$$k_{y\ell} = \frac{\ell-1}{L_y} \qquad \ell = 1(1)\frac{N_y}{2}$$

The expressions above are composed of the double sum of complex harmonics where $A_{j\ell}$ are complex Fourier coefficients. The length of the grid in the x and y directions is denoted by L_x, L_y, respectively, while the number of data points in the x and y directions is denoted by N_x and N_y, respectively.

number of data points in the x and y directions is denoted by N_x and N_y, respectively.

The sample temperature variance can be written as

$$\sigma_T^2 = \frac{1}{N_x N_y} \sum_x \sum_y (T[x,y] - \bar{T})^2 \qquad (3)$$

where $\bar{T}$ is the sample mean. The sample mean is

$$\bar{T} = \frac{1}{N_x N_y} \sum_x \sum_y T(x,y) \quad . \qquad (4)$$

More importantly, the sample temperature variance can be written as

$$\sigma_T^2 = \sum_j \sum_\ell \frac{|A_{j\ell}|^2}{4} \qquad (5)$$

In the above equation the temperature variance is expressed in terms of a sum of the squares of the complex amplitudes.

The SST variance spectrum is proportional to $|A_{j\ell}|^2$ and represents a partitioning of the temperature variance in wavenumber space. The symbol $E_T(\hat{k})$ will represent this partitioning and will be referred to as the two-dimensional temperature variance spectrum. [The dimensions of $E_T(\hat{k})$ are LT^2 since $E_T(\hat{k})$ has units of variance of temperature (T^2) divided by wavenumber (L^{-1}).]

The temperature wavenumber variance spectrum can always be defined as a separation into an isotropic part and an anisotropic part. This separation is expressed in the following formula

$$E_T(\hat{k}) = E_1(|\hat{k}|) + E_2(\hat{k}) \quad . \qquad (6)$$

E_1 is the isotropic part, which does not depend on direction, and E_2 is the anisotropic part which does depend on direction. The wavenumber vector $\hat{k}$ is defined

$$\hat{k} = k_x + ik_y \quad . \qquad (7)$$

This complex variable can be written

$$\hat{k} = k_x + ik_y \quad . \qquad (7)$$

This complex variable can be written

$$\hat{k} = |\hat{k}| e^{i\theta} \qquad (8)$$

which is a function of the wavenumber, $|\hat{k}|$, and a phase angle, θ.

If we integrate the two-dimensional temperature variance spectrum over all phase angles we have as shown

$$\frac{1}{2\pi} \int_{-\pi}^{\pi} E_T(|\hat{k}|e^{i\theta})\, d\theta = E_1(|\hat{k}|) \ . \tag{9}$$

Recall that $E_1(|\hat{k}|)$ is the isotropic part of the temperature variance spectrum. Because this is true, we can go back to (6) and see that

$$\int_{-\pi}^{\pi} E_2\,(\hat{k})\, d\theta = 0 \ . \tag{10}$$

In our spectral study we are not dealing with a continuous field; instead, we are dealing with discrete points. For the case of a field of discrete points, a discrete sum must be employed in expressing the isotropic part of the temperature variance spectrum. This discrete sum can be written as

$$\frac{1}{N} \sum_{j} \sum_{\ell} E_{T_{j\ell}}(|\hat{k}|e^{i\theta}) = E_1(|\hat{k}|) \tag{11}$$

where j and ℓ are chosen such that $|k_{xj} + ik_{y\ell}| \in |\hat{k}| \pm \delta|\hat{k}|$.

Fig. 13b shows graphically the summing method that was employed. In this figure values of k_x range from 0 to 1/2 km^{-1} and the values of k_y range from 0 to 1/2 km^{-1}. If a contribution, $E_{T_{j\ell}}$, to the isotropic part of the temperature variance spectrum falls within a certain wavenumber range $|\hat{k}| \pm \delta|\hat{k}|$ it is summed in with all other contributions which fall within this range. The sum of all of the contributions to the isotropic part of the temperature variance spectrum is then divided by N the number of contributions. The fact that we are computing the

the isotropic part of the temperature variance spectrum is then divided by N the number of contributions. The fact that we are computing the isotropic part of the temperature variance spectrum by this method is

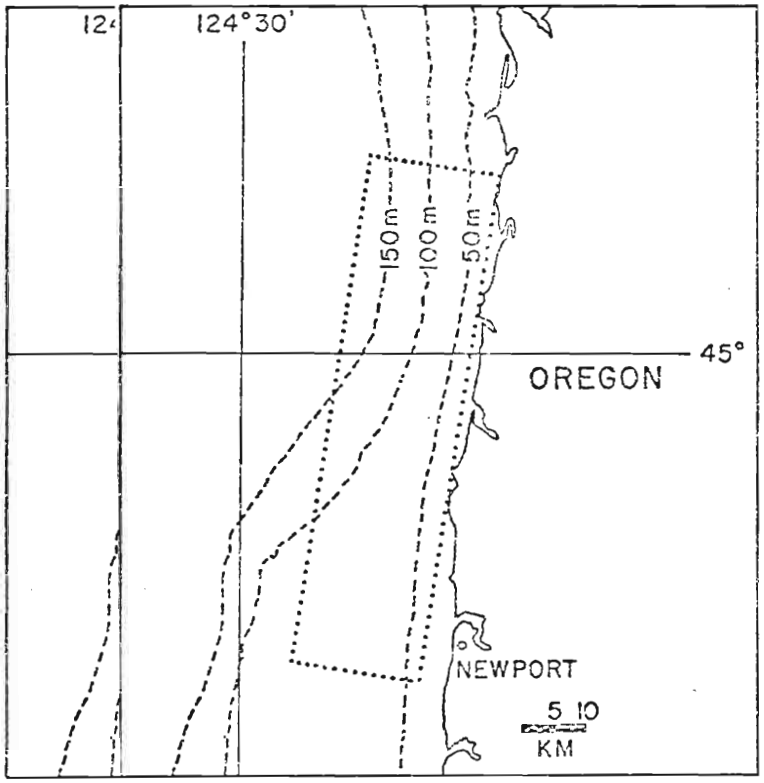

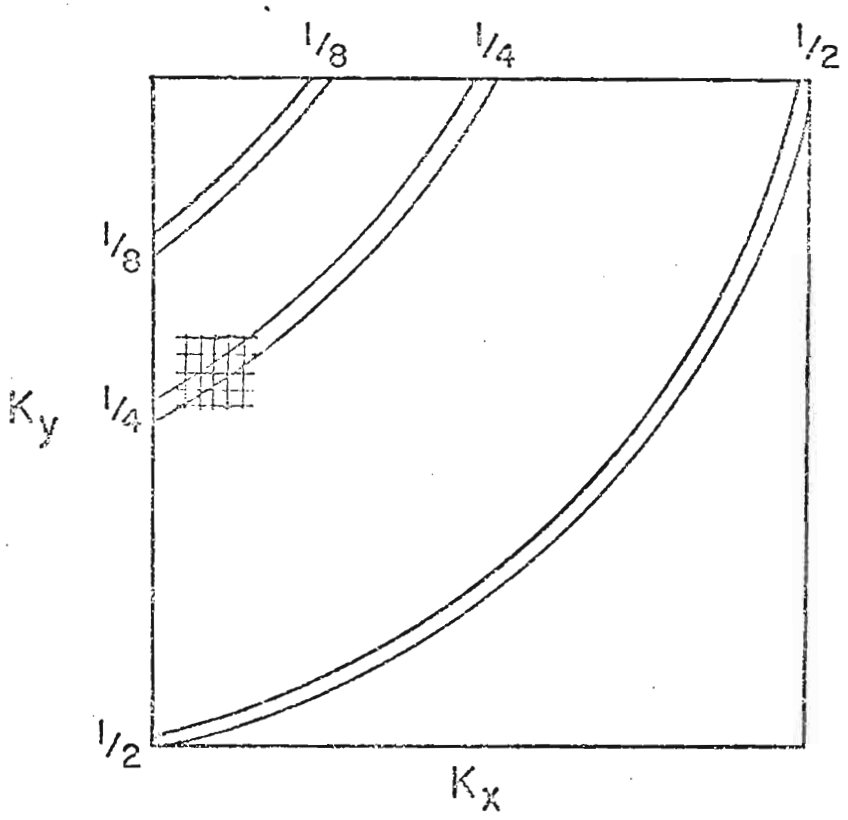

Fig. 13. (a) Schematic diagram of the rotated rectangular grid which contained the SST values values from which the spectra were computed. (b) Schematic diagram of summation method for findingfinding isotropic temperature variance spectrum.

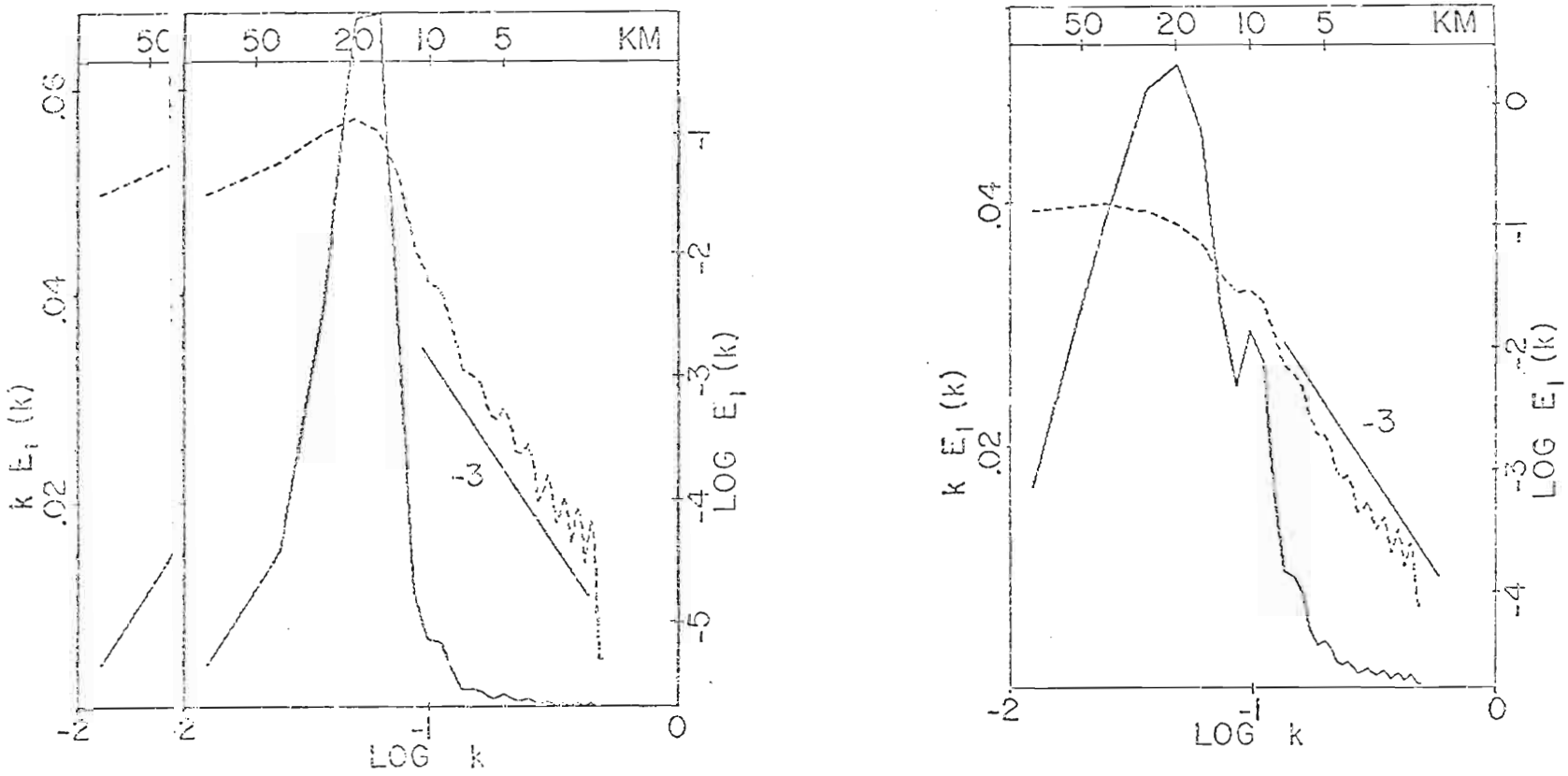

Fig Fig. 14. Graphic results of spectral analysis for (a) 14 July, 1973, horizontal sea surface teface temperature field and (b) 15 July, 1973, horizontal sea surface temperature field. Solid lineld line represents plot of $kE_1(k)$ vs. log k. Dashed line represents plot of log $E_1(k)$ vs. log k. log k. Solid line labelled -3 represents -3 slope.

important as we shall see later.

Fig. 14a shows a graph of one of the computed spectra. This graph refers to a spectrum computed from the horizontal SST field on 14 July. (The horizontal SST and perturbation maps for 14 July are shown in Fig. A-14.) The solid line in the graph refers to a plot of wavenumber times the isotropic temperature variance spectrum vs. the log of wavenumber. This plot has the advantage that area under the curve represents the sample variance. From this plot we can see that there is a large contribution to the variance in the range of wavelengths from 16-20 km. The dotted line represents a plot of log of the isotropic temperature variance spectrum vs. log of wavenumber. In this log-log plot we note a steep slope toward high wavenumbers. From comparison with the solid line labelled -3 we can see that in the wavenumber region from $1/15$ km^{-1} to $1/4$ km^{-1} there is an approximate slope of -3. A glance at Fig. 14b reveals basically the same results as those discussed in connection with Fig. 14a. Fig. 14b shows the results of a spectral analysis of horizontal SST for 15 July (see Fig. A-15 for horizontal SST map and perturbation map). A spectral peak exists at the 20 km wavelength and there is a large contribution to the variance in the wavelength range of 16-27 km. From the dotted line representing the log-log plot, again note the approximate -3 slope this time in the wavenumber range $1/20$ km^{-1} to $1/4$ km^{-1}. A third graph depicting the results from a spectral analysis of 16 July SST data is shown in Fig. 15a. As observed in the previous figure, a spectral peak is located at the 20 km wavelength

tral analysis of 16 July SST data is shown in Fig. 15a. As observed in the previous figure, a spectral peak is located at the 20 km wavelength

and in the wavelength range of 16-27 km a large contribution to the variance exists. An approximate -3 slope can also be seen from the

log-log plot. A two-dimensional planar trend was removed during the spectral analysis of the daily SST data. As mentioned earlier in this section, spectra were computed from the daily perturbations from the three-week means. One of the results from these calculations is shown in Fig. 15b which represents a graph of spectral results from perturbation data for 14 July. Note from comparison with the dotted line and the solid line labelled -3 an approximate -3 slope. We chose to show the results of our spectral analyses for 14, 15, and 16 July because on these days the mesoscale sea surface temperature field displayed a large amount of variability.

The plots of $kE_T(k)$ vs. the logarithm of wavenumber k consistently revealed a spectral peak in the wavelength range 16-40 km. A peak at 16-20 km is significant and not an artifact of the limited observational region. A peak at 40 km is suspect due to the limited size. As for the log-log plots, a glance at Fig. 16 can reveal the consistency of the -3 slope for spectra computed from the daily horizontal SST field. Fig. 16 is a scatter diagram which represents a composite of 16 days of computed spectra from 16 days of SST data. Each day's spectrum was computed and then normalized by that day's variance and then a composite of the log-log plots was constructed. An approximate -3 slope in the range of wavenumber 1/20 to 1/4 km^{-1} is easily seen. From this graph we conclude that the isotropic sea surface temperature variance spectrum follows a power law of -3.

We also did some calculations of the one-dimensional temperature follows a power law of -3.

We also did some calculations of the one-dimensional temperature spectra from our SST data. The results from these calculations indicated a k^{-p} dependence of the spectra which was comparable to that found by

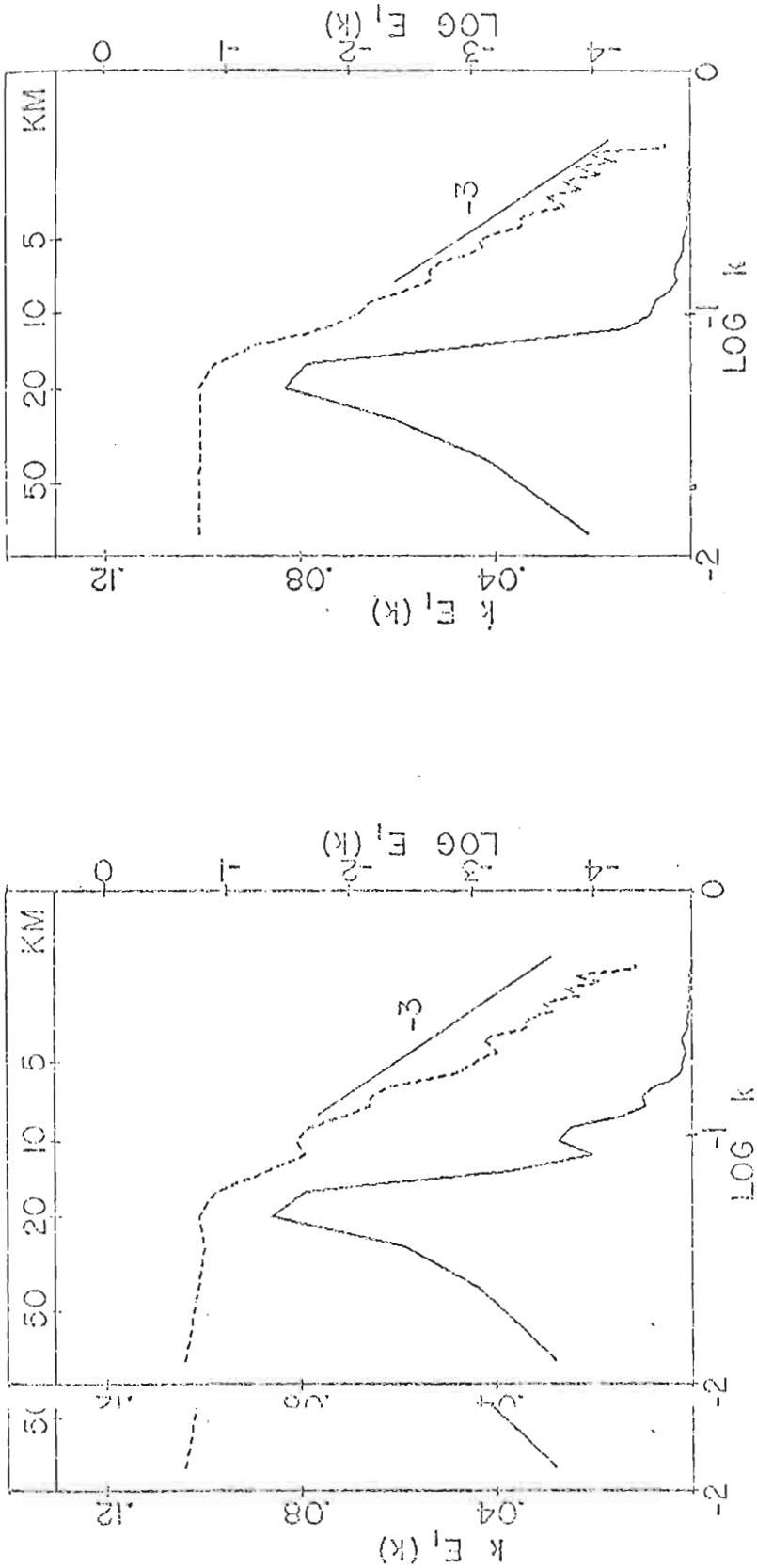

Fig. 15. Same as Fig. 14, but for (a) 16 July, 1973, horizontal SST field, and (b) 14 July, 1973, perturbation field.

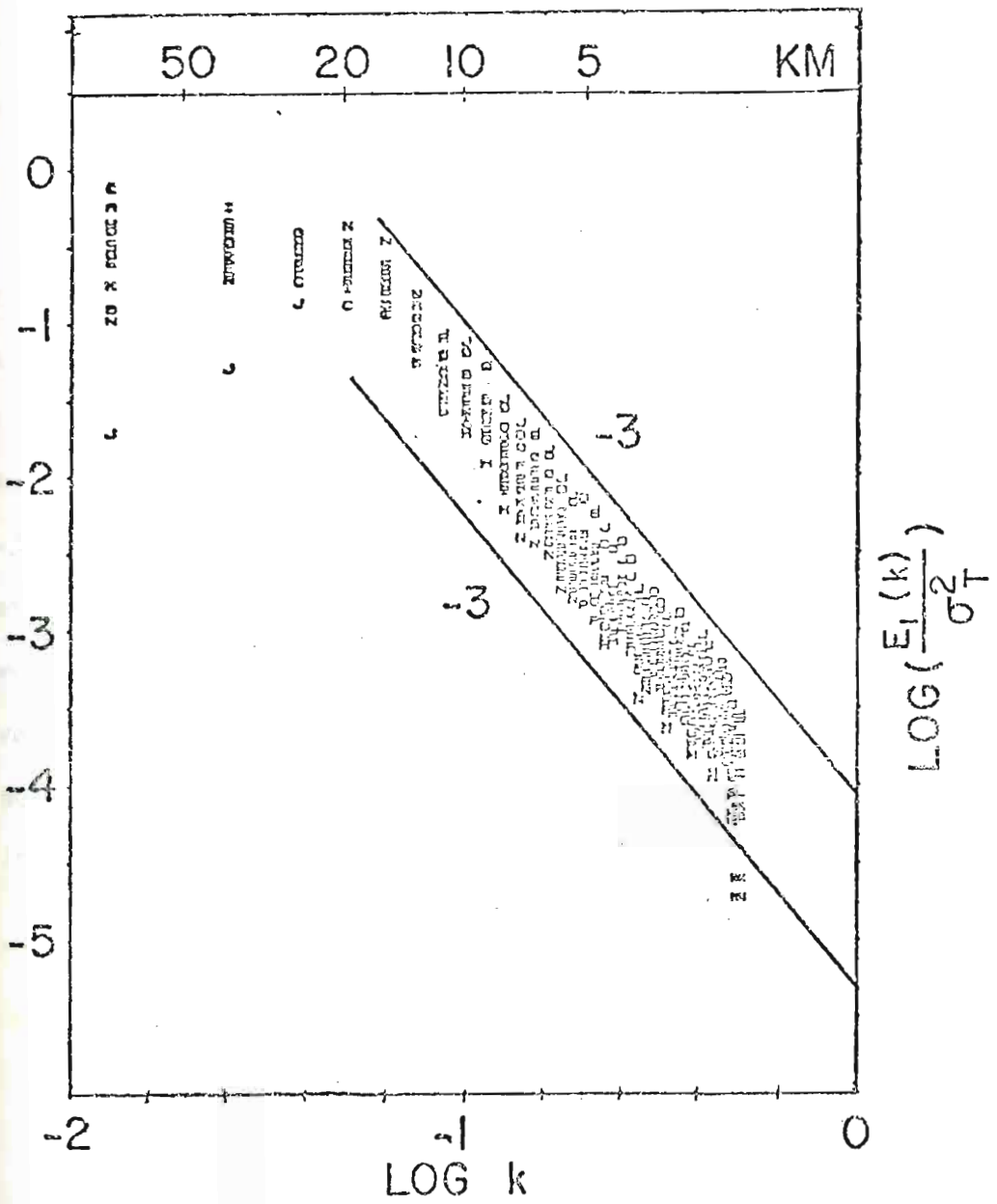

Fig. 16. Scatter diagram representing a composite of sixteen log-log plots of the normalized isotropic temperature variance spectrum vs. wavenumber. Each of the sixteen plots is a graphic representation of a daily spectrum. These spectra were computed for SST gathered during the period 27 June to
sixteen log-log plots of the normalized isotropic temperature variance spectrum vs. wavenumber. Each of the sixteen plots is a graphic representation of a daily spectrum. These spectra were computed for SST gathered during the period 27 June to
16 July, 1973. The solid lines represent -3 slopes.

Saunders (1972). Isotropy is assumed in the computation of the one-dimensional spectra; whereas, when we computed spectra from the two-dimensional SST field we only considered the isotropic part of the temperature variance spectrum.

Charney indicated in his paper that his predicted k^{-3} behavior for the temperature variance might apply to oceanic fields in regions of strong baroclinicity. His prediction assumes isotropy. At the time (1971) no observations were available for comparison with his theory. An interesting note is that Lilly and Lester (1974) found an approximate -3 slope in a mesoscale wavelength (3-20 km) for spectra computed from atmospheric temperature data. We conclude this section by stating that we have found a k^{-3} behavior of the isotropic sea surface temperature variance spectrum in the mesoscale wavelength range of 4-20 km. We do not, however, imply that, therefore, the geostrophic turbulence theory is applicable.

6. SUMMARY AND CONCLUSIONS

Some results of an investigation of the nature of the mesoscale variability of SST off the central coast of Oregon are presented in this paper. Our investigation of this mesoscale variability of SST is based on the extensive amount of SST data gathered during the two-month long COHO project in 1973. Basically, we found that the mesoscale SST field off the coast of Oregon is highly variable from day to day and point to point.

We investigated the response of the SST field to wind forcing. We found that SST are generally cooler when northerlies are blowing and warmer when southerlies are blowing. SST may lower rapidly within several days during periods of moderate to strong northerly winds. Upwelling caused by these northerly winds accounts for the lower SST during these periods. This is, of course, to be expected.

In the present study we only considered the influence of the wind field on the SST field. The wind field does seem to dominate the SST field. Future research studies of large amounts of mesoscale SST data gathered by remote sensing techniques could investigate the effects of solar heating, precipitation, cloud cover, and differences in temperature between lands and seas. Also not considered in this study were relations between the daily surface current and the mesoscale SST field. Although not considered in this paper, a strong feedback may exist between change in the SST field and the sea breeze (Johnson and O'Brien, 1973).

between the daily surface current and the mesoscale SST field. Although not considered in this paper, a strong feedback may exist between change in the SST field and the sea breeze (Johnson and O'Brien, 1973).

An investigation of the daily horizontal SST maps revealed the location of areas of strong horizontal SST gradients called oceanic fronts. By examining perturbation maps, the location of these fronts is easily determined. These oceanic fronts represent a zero order discontinuity in SST. Often rather well-defined, these fronts are usually easily visible from a low altitude aircraft. Because these fronts concentrate phytoplankton and other buoyant material, they are important biologically as well as physically.

From maps of the perturbations from the three-week means, we observed large numbers of eddies in the mesoscale SST field. Individual eddies are not easily traced from day to day because of the strong horizontal flow and strong shear in the longshore current. In order to determine the scales of the eddies in the horizontal temperature field in the upwelling zone quantitatively, a spectral study of the SST data was undertaken. The results from this two-dimensional spectral analysis indicated that a large amount of the variance of the SST was concentrated in the 16-40 km wavelength range. This result leads us to conclude that a large amount of the variance of the SST is concentrated in mesoscale eddies which are being advected through the upwelling region.

From our spectral analysis, we also found that over the range of the scales from 4-20 km the isotropic part of the temperature variance spectrum obeyed a -3 power law. Charney's (1971) theory is candidate to explain this power law physically. Several other investigators have found approximate -3 spectral slopes from observed temperatures in the

explain this power law physically. Several other investigators have found approximate -3 spectral slopes from observed temperatures in the atmosphere.

A study of the three-week mean sea surface temperature fields

indicated that the mean isotherms tended to follow the large-scale bathymetry.

In this paper, we have presented the results of an analysis of the most extensive gathering of SST in a coastal upwelling zone to date. Hopefully, the results of this analysis have provided an insight into the understanding of the nature of the mesoscale SST field in an upwelling zone and will provide the basis for additional research.

APPENDIX A

A TIME SERIES OF SST MAPS

This appendix contains 16 days of horizontal sea surface temperature maps and the corresponding daily perturbations from the three-week mean temperatures for each of these 16 days. This series of maps begins on 27 June and ends on 16 July (20 day period with 4 days of maps unavailable because fog prevented the mapping flights). This period of days corresponds to the first three-week period mentioned in Section 3 from which means and perturbations from the means were computed. Two upwelling events separated by several days of southerly winds occurred during this three-week period. Each horizontal SST or perturbation map contains either the horizontal SST or perturbations in degrees C and the inshore bathymetry curves for 50, 100, and 150 m in the COHO flight region.

Horizontal sea surface temperatures in the inshore 10 km ranged from less than 8C all alongshore on 12 July (Fig. A-13a) to greater than 14C alongshore northward from Depoe Bay to Cape Lookout on 6 July (Fig. A-9a). Horizontal sea surface temperatures varied from less than 8C inshore of the 50 m isobath to greater than 13C offshore of the 150 m isobath on 12 July (Fig. A-13a) the day when the coolest SST were observed in the flight region. On 7 July (Fig. A-10a) which was one of the days when measured SST were warmest, SST greater than 15C were observed in most of the flight region.

The daily perturbation maps for this three-week period reveal the

mesoscale variability of the SST. In order to compute the daily perturbations from the mean at every point on the map, the mean temperature at every point is subtracted from the daily temperature at every point. Daily perturbations of ±3C from the three-week mean were not uncommon inshore of the 100 m isobath. As was discussed earlier in Section 3, strong horizontal flow (10-40 cm sec^{-1}) in the mapping area prevents the tracing of individual eddies from day to day. A glance at the perturbation maps for 14, 15 and 16 July (Figs. A-14b, A-15b, A-16b) and a comparison of these maps with their respective horizontal SST maps shows that the perturbation field can reveal the existence and location of the oceanic fronts in the mapping region.

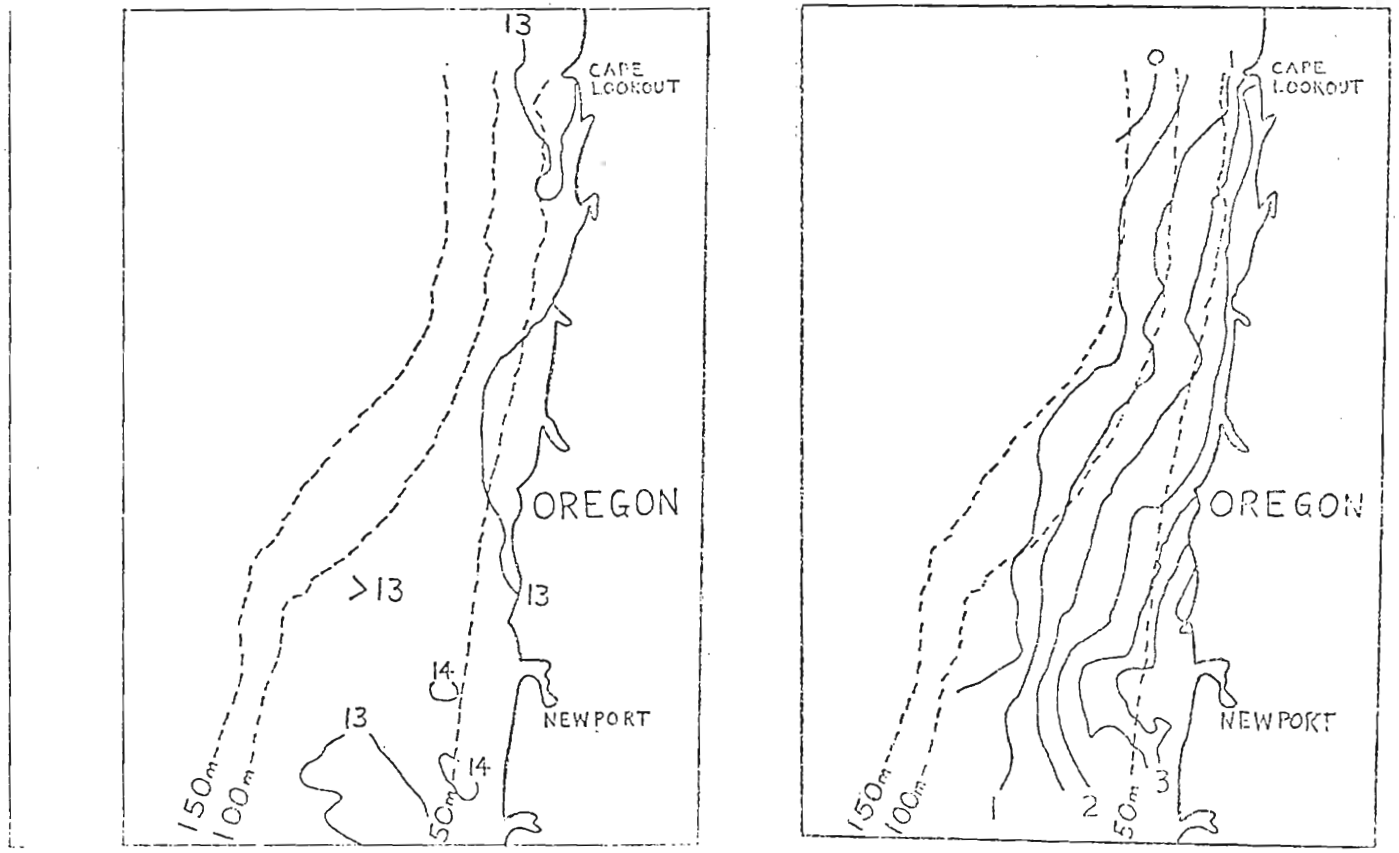

Fig. A-1. (a) Horizontal sea surface temperatures, and (b) perturbations fr from the three-week mean in the COHO flight region for 27, 1973.

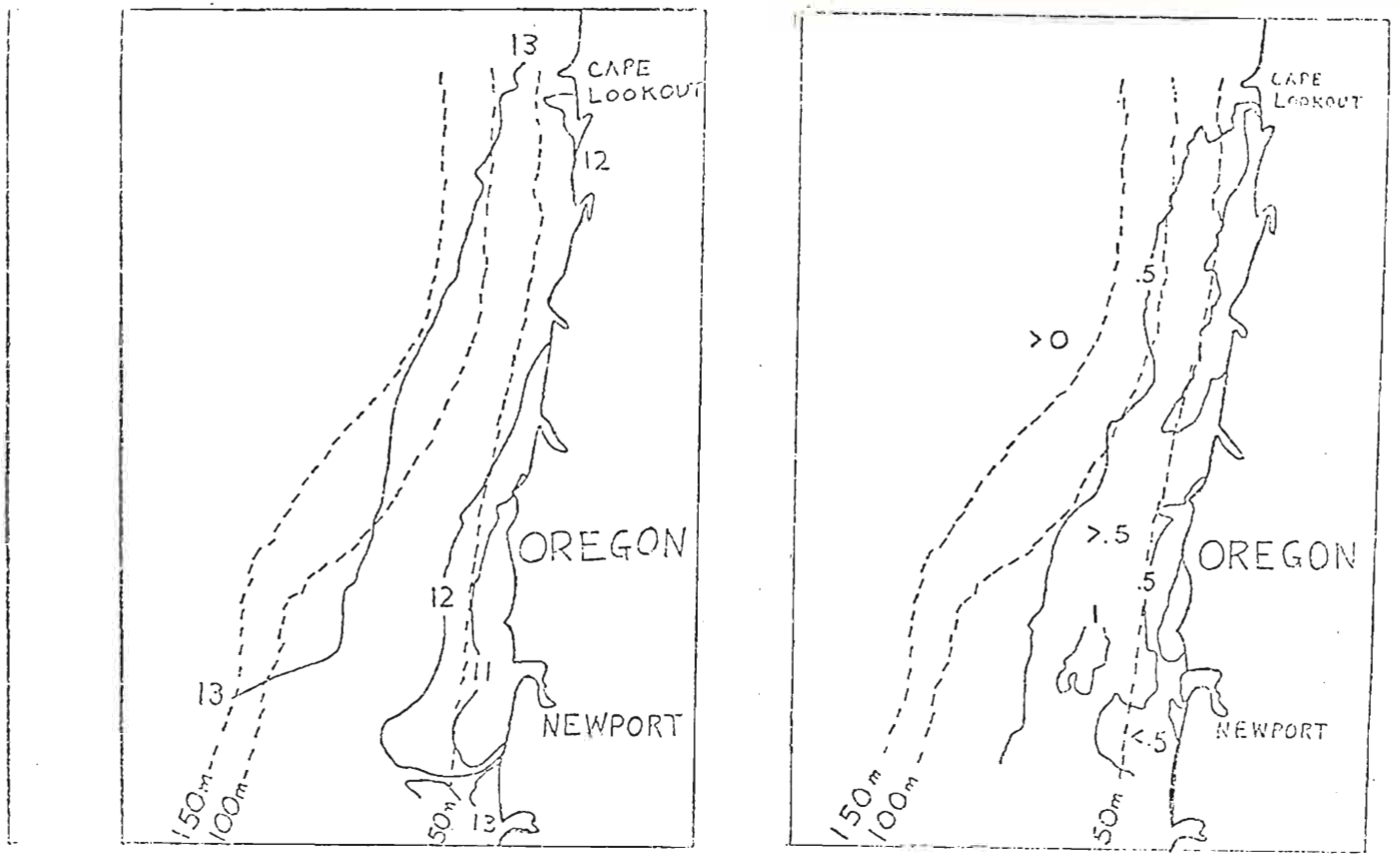

Fig. A-2. (a) Horizontal sea surface temperatures, and (b) perturbations from the three-week mean in the COHO flight region for 28 June, 1973.

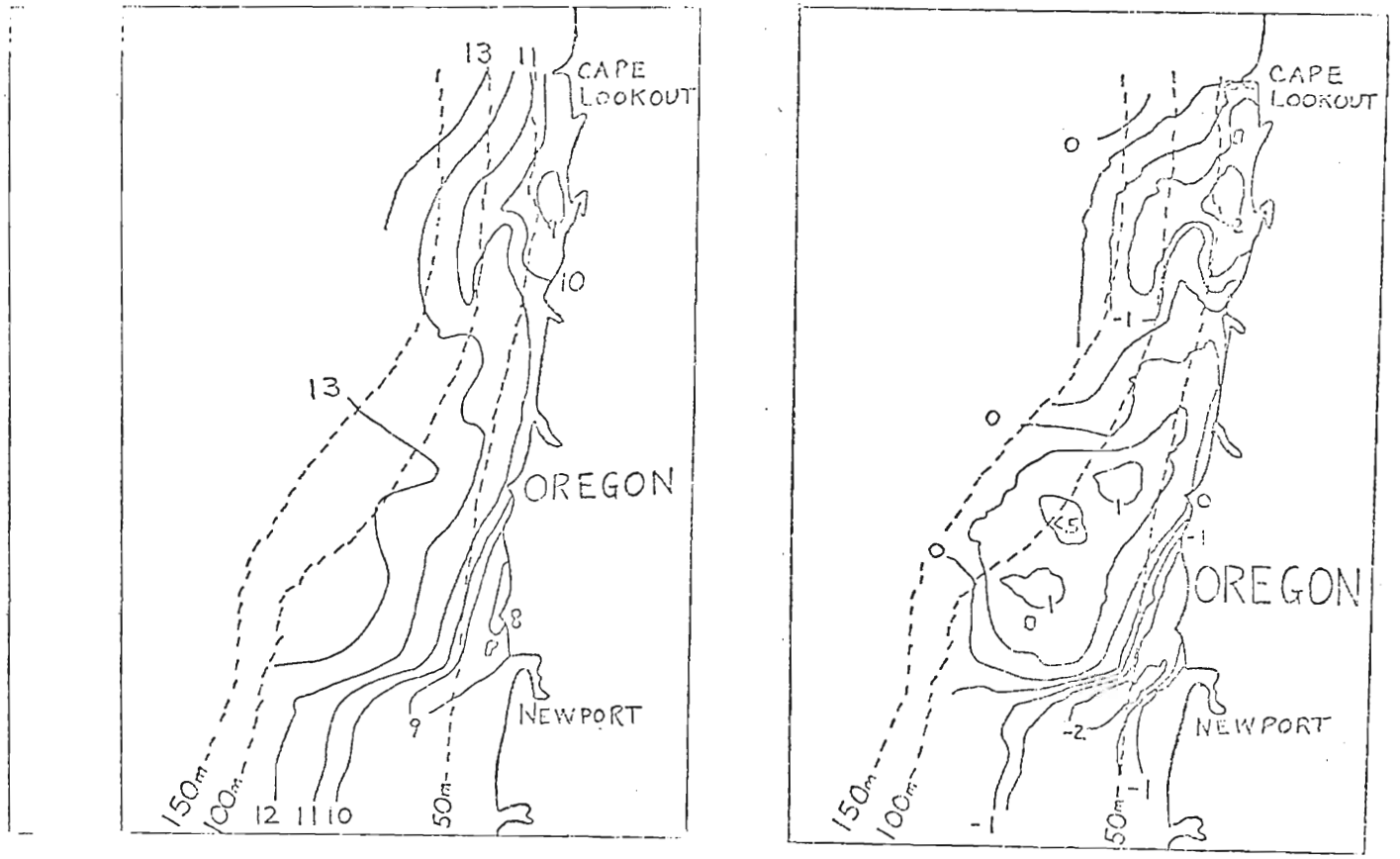

Fig. A-3. (a) Horizontal sea surface temperatures, and (b) perturbations from the three-week mean in the COHO flight region for 29 June, 1973.

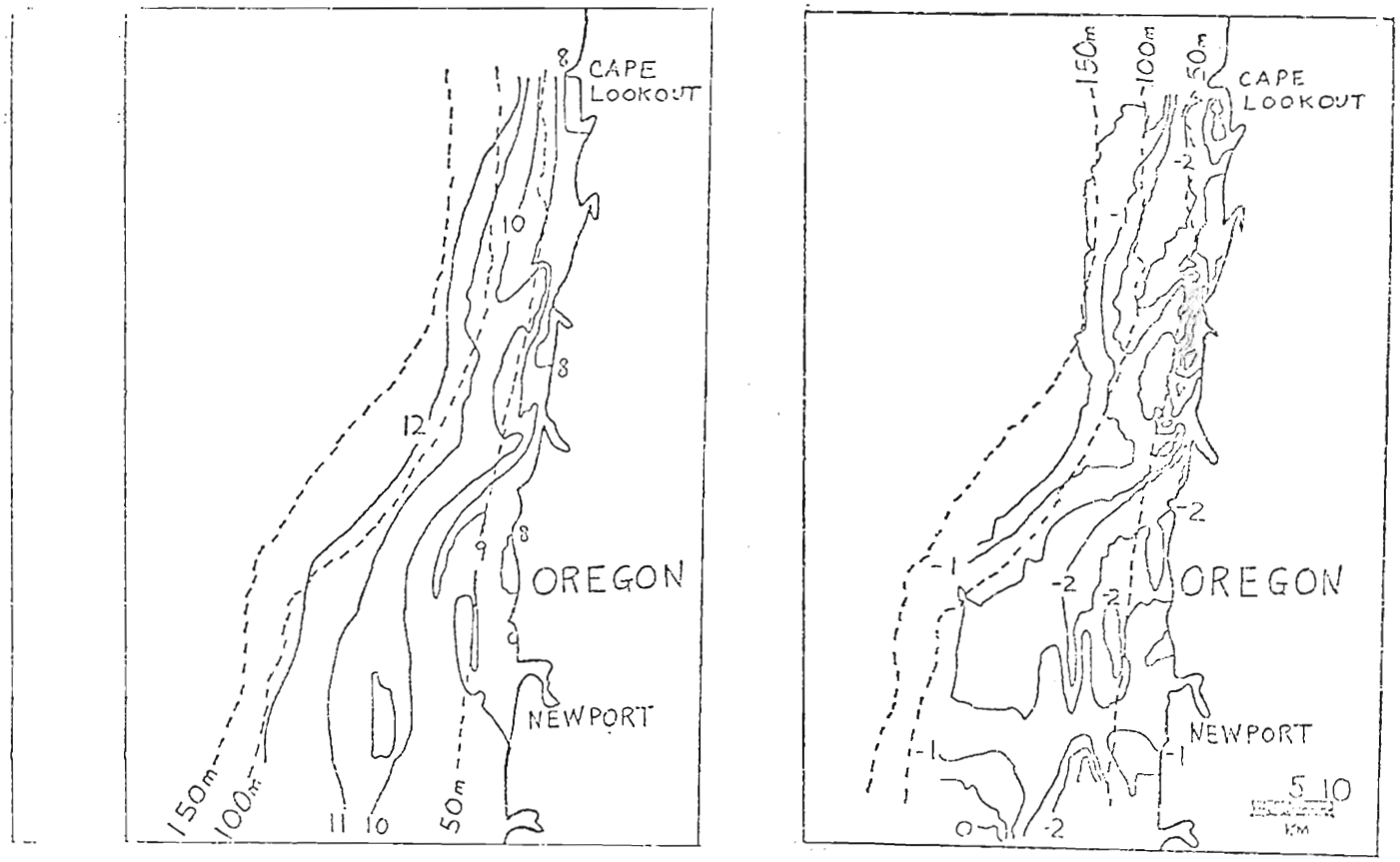

Fig. A-4. (a) Horizontal sea surface temperatures, and (b) perturbations from the three-week mean in the COHO flight region for 30 June, 1973.

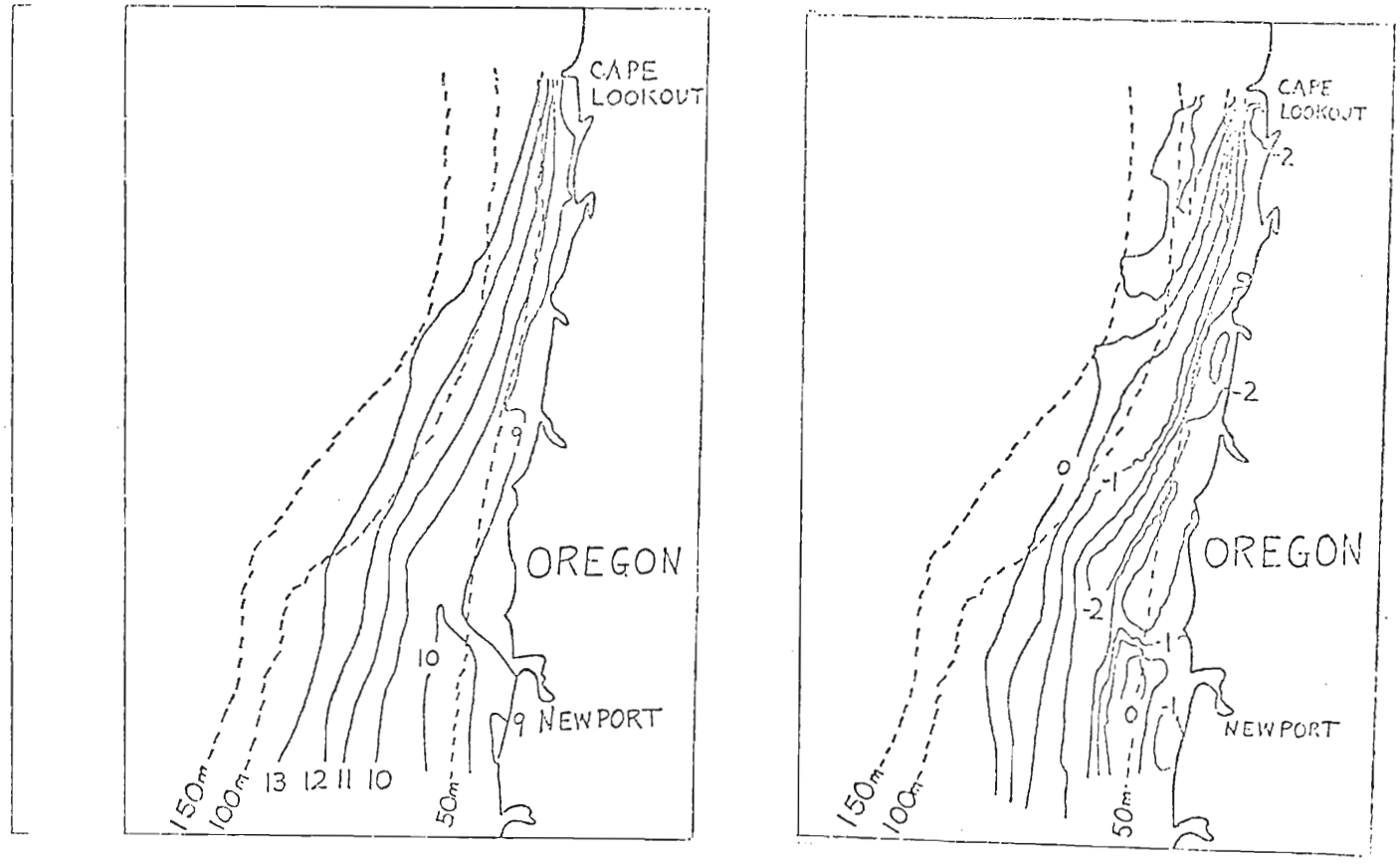

Fig. A-5. (a) Horizontal sea surface temperatures, and (b) perturbations from the three-week mean in the COHO flight region for 1 July, 1973.

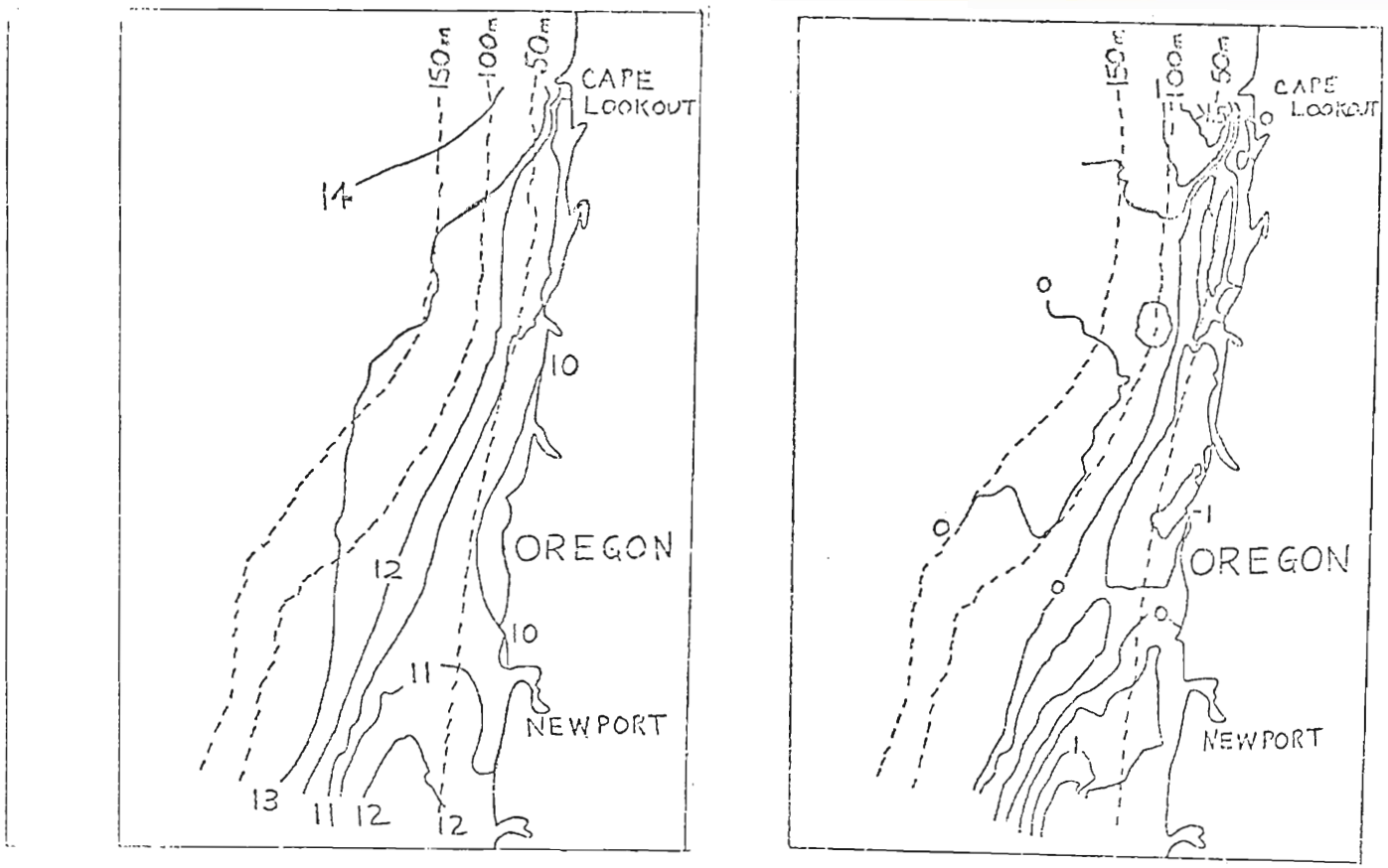

Fig. A-6. (a) Horizontal sea surface temperatures, and (b) perturbations from the three-week mean in the COHO flight region for 2 July, 1973.

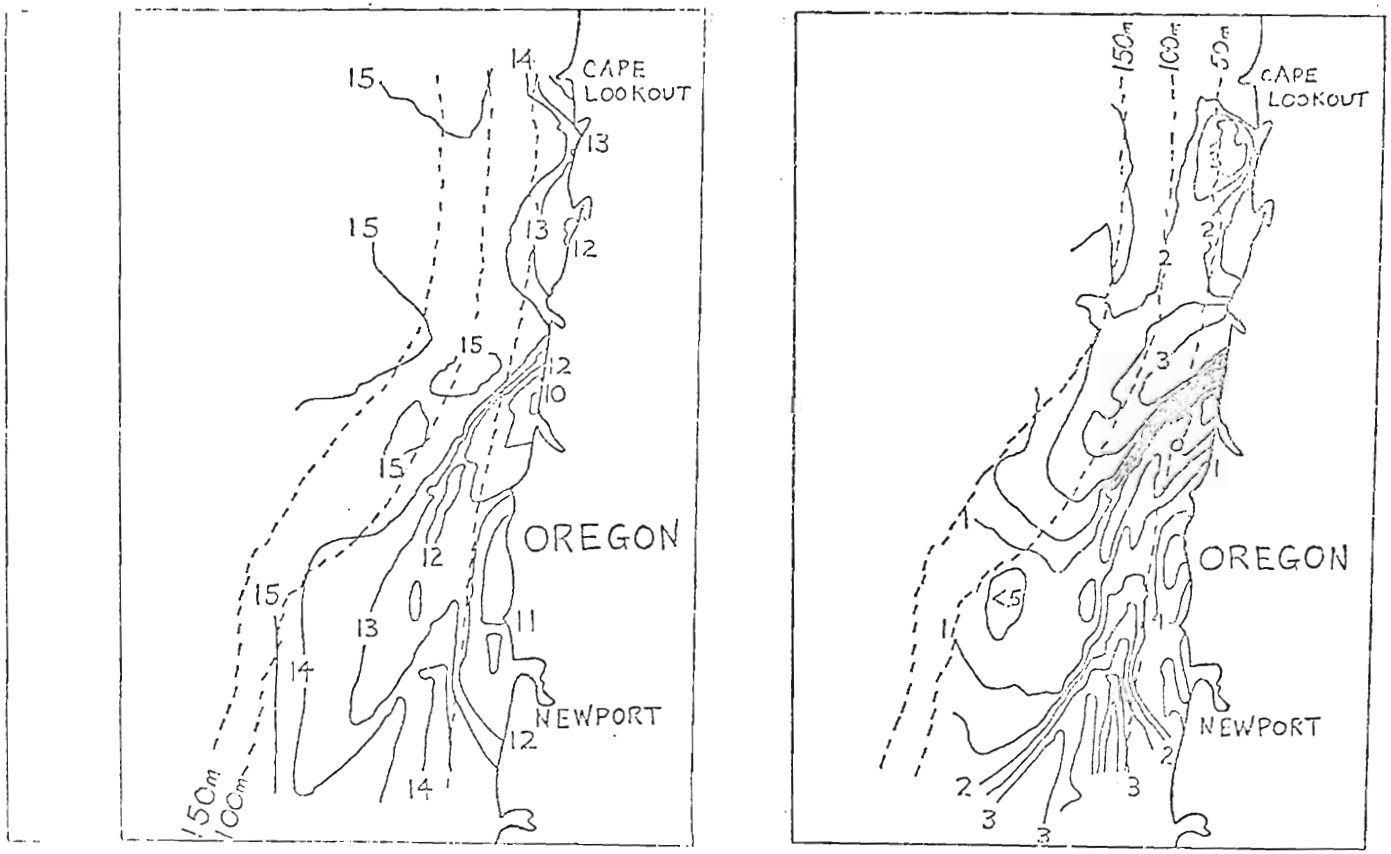

Fig. A-7. (a) Horizontal sea surface temperatures, and (b) perturbations from the three-week mean in the COHO flight region for 3 July, 1973.

tic

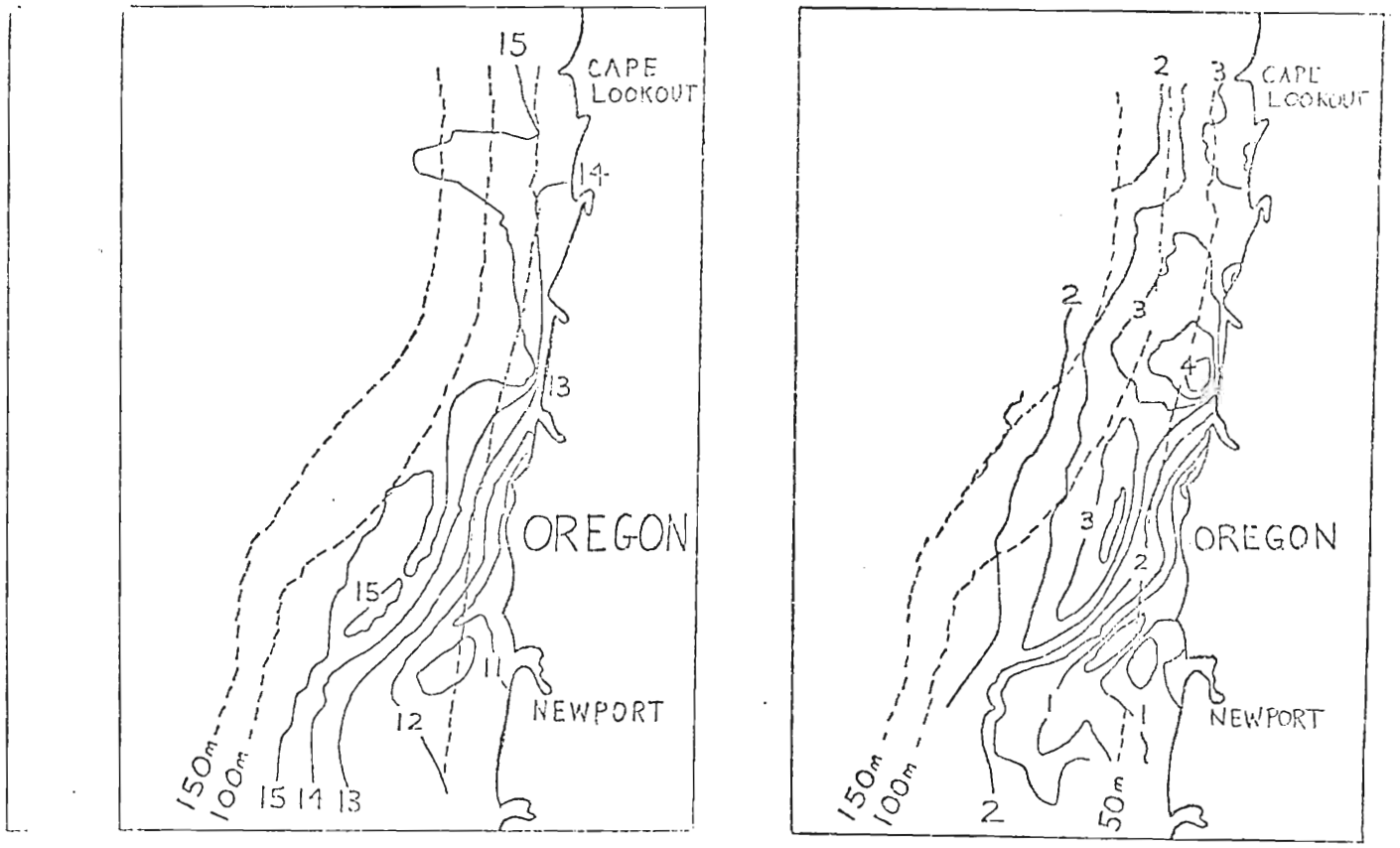

Fig. A-8. (a) Horizontal sea surface temperatures, and (b) perturbations from the three-week mean in the COHO flight region for 5 July, 1973.

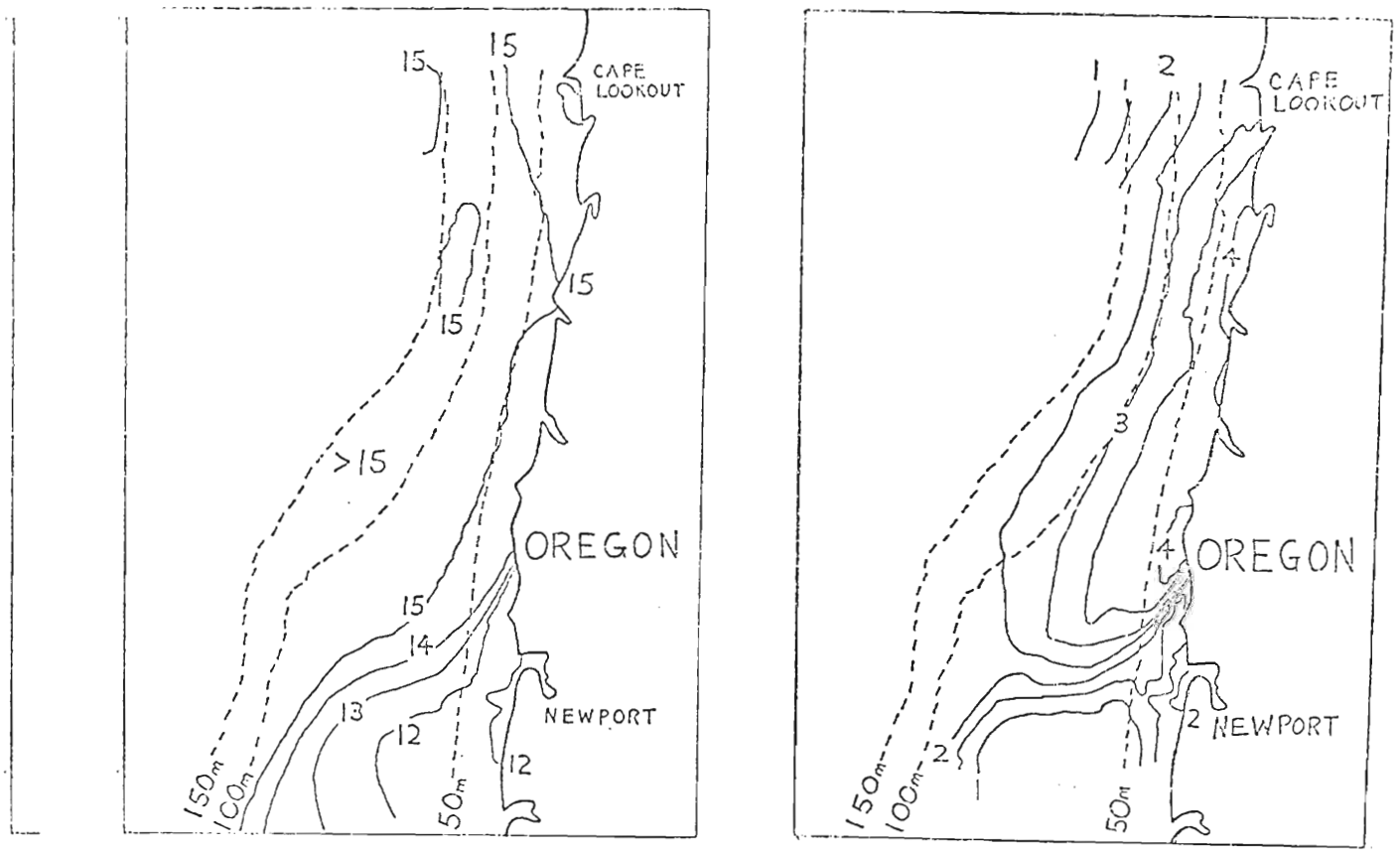

Fig. A-9. (a) Horizontal sea surface temperatures, and (b) perturbations from the three-week mean in the CCHO flight region for 6 July, 1973.

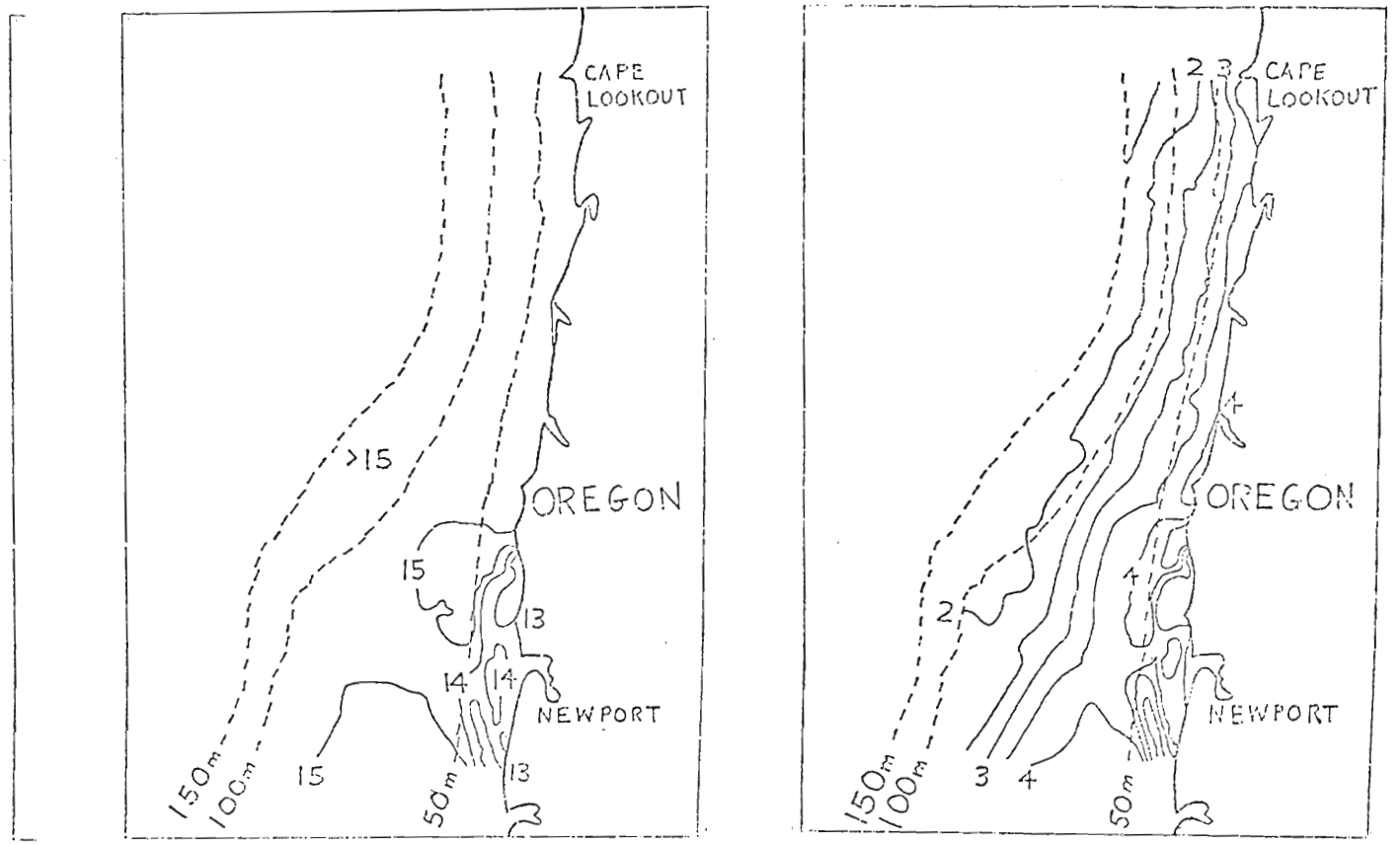

Fig. A-10. (a) Horizontal sea surface temperatures, and (b) perturbations from the three-week mean in the CCHO flight region for 7 July, 1973.

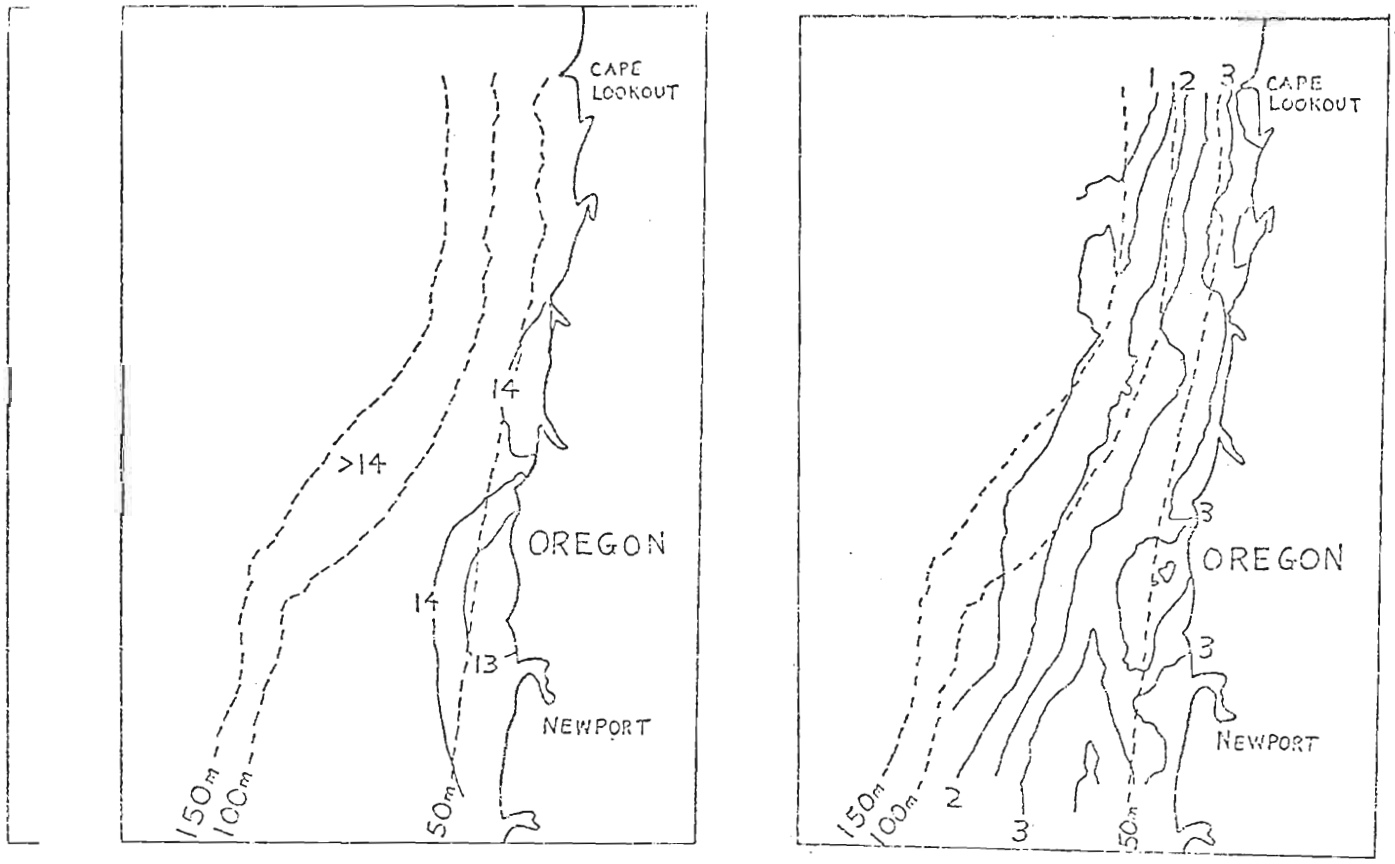

Fig. A-11. (a) Horizontal sea surface temperatures, and (b) perturbations from the three-week mean in the CCHO flight region for 9 July, 1973.

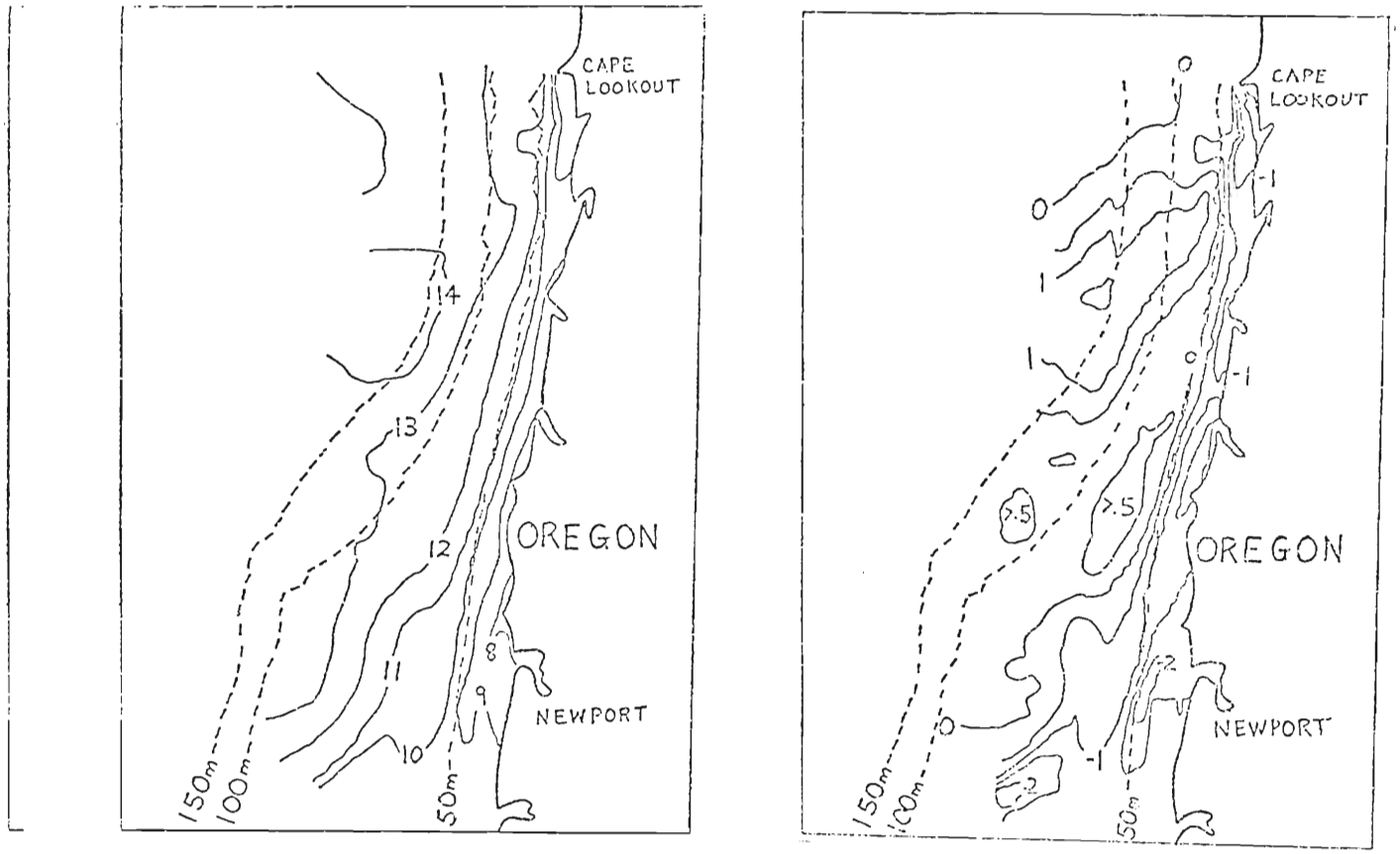

Fig. A-12. (a) Horizontal sea surface temperatures, and (b) perturbations from the three-week mean in the COHO flight region for 11 July, 1973.

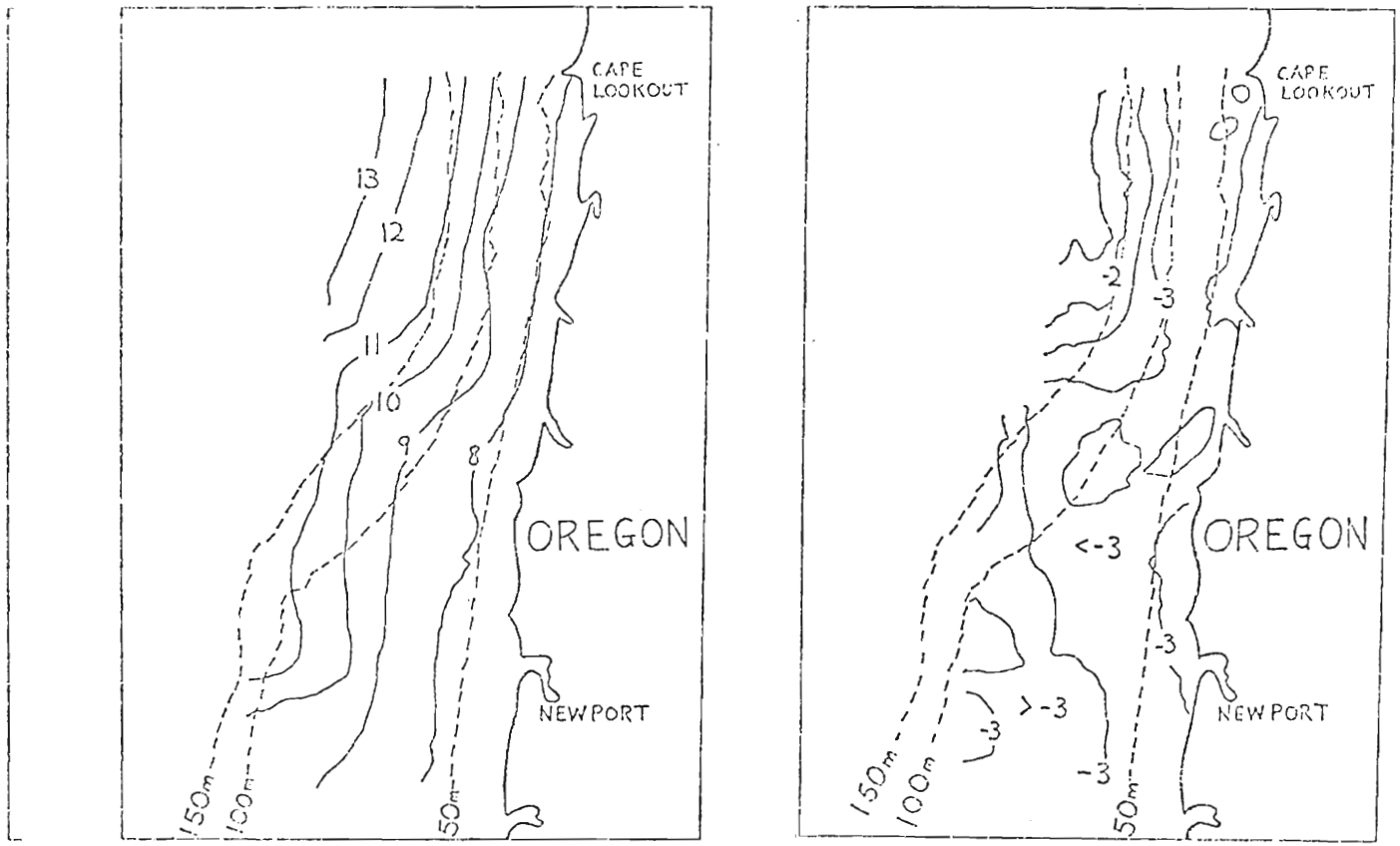

Fig. A-13. (a) Horizontal sea surface temperatures, and (b) perturbations from the three-week mean in the COHO flight region for 12 July, 1973.

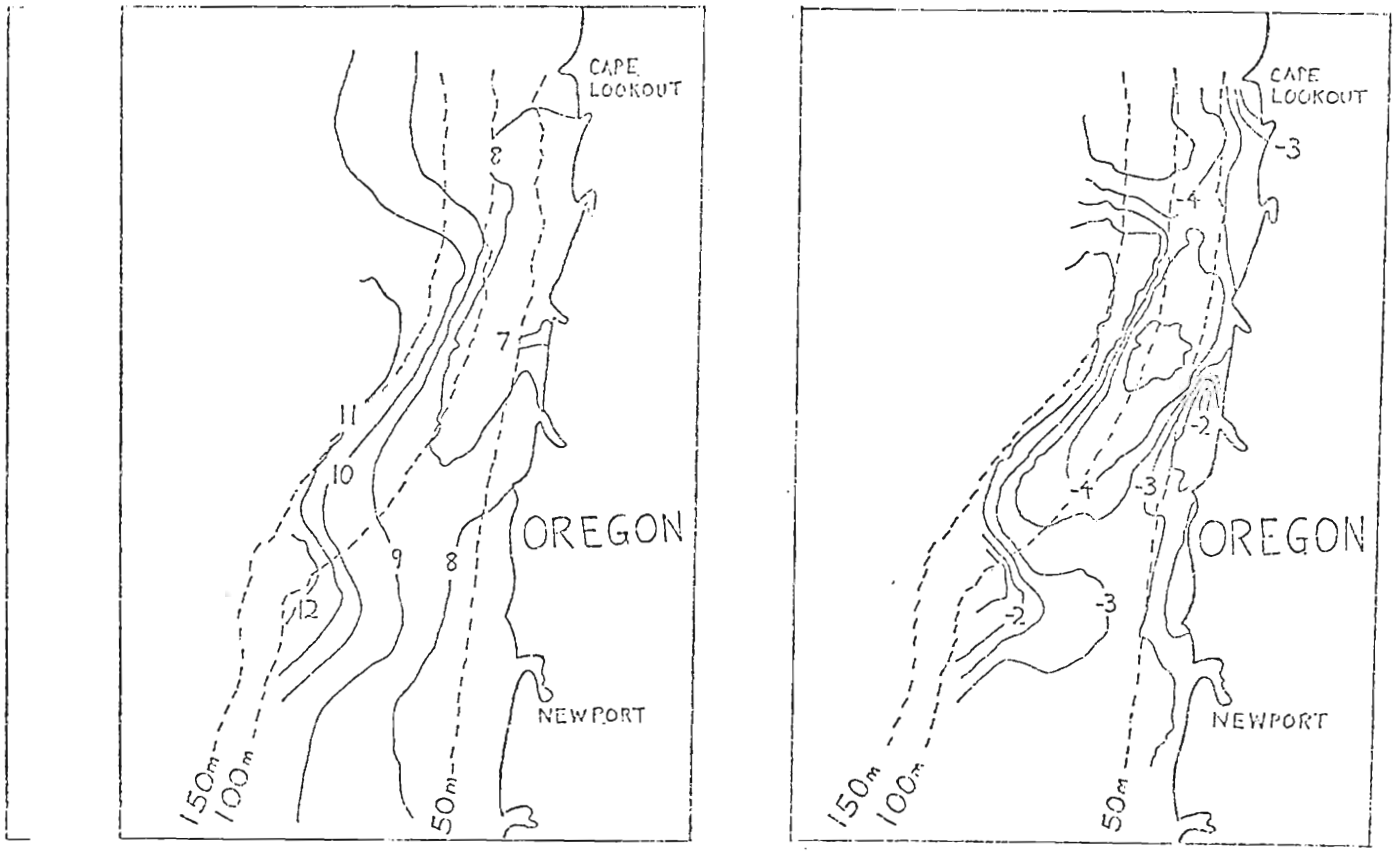

Fig. A-14. (a) Horizontal sea surface temperatures, and (b) perturbations from the three-week mean in the COHO flight region for 14 July, 1973.

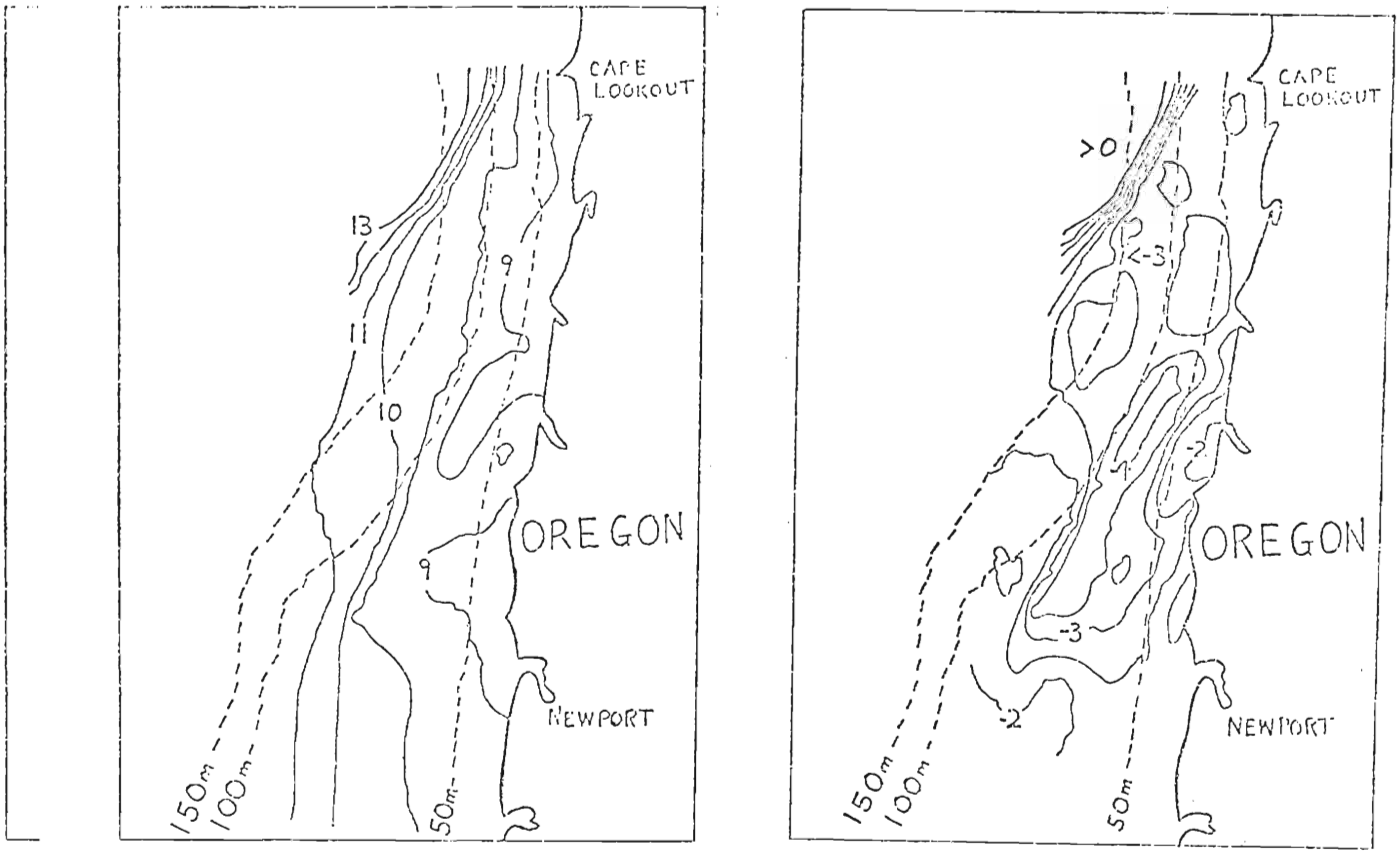

Fig. A-15. (a) Horizontal sea surface temperatures, and (b) perturbations from the three-week mean in the COHO flight region for 15 July, 1973.

tic

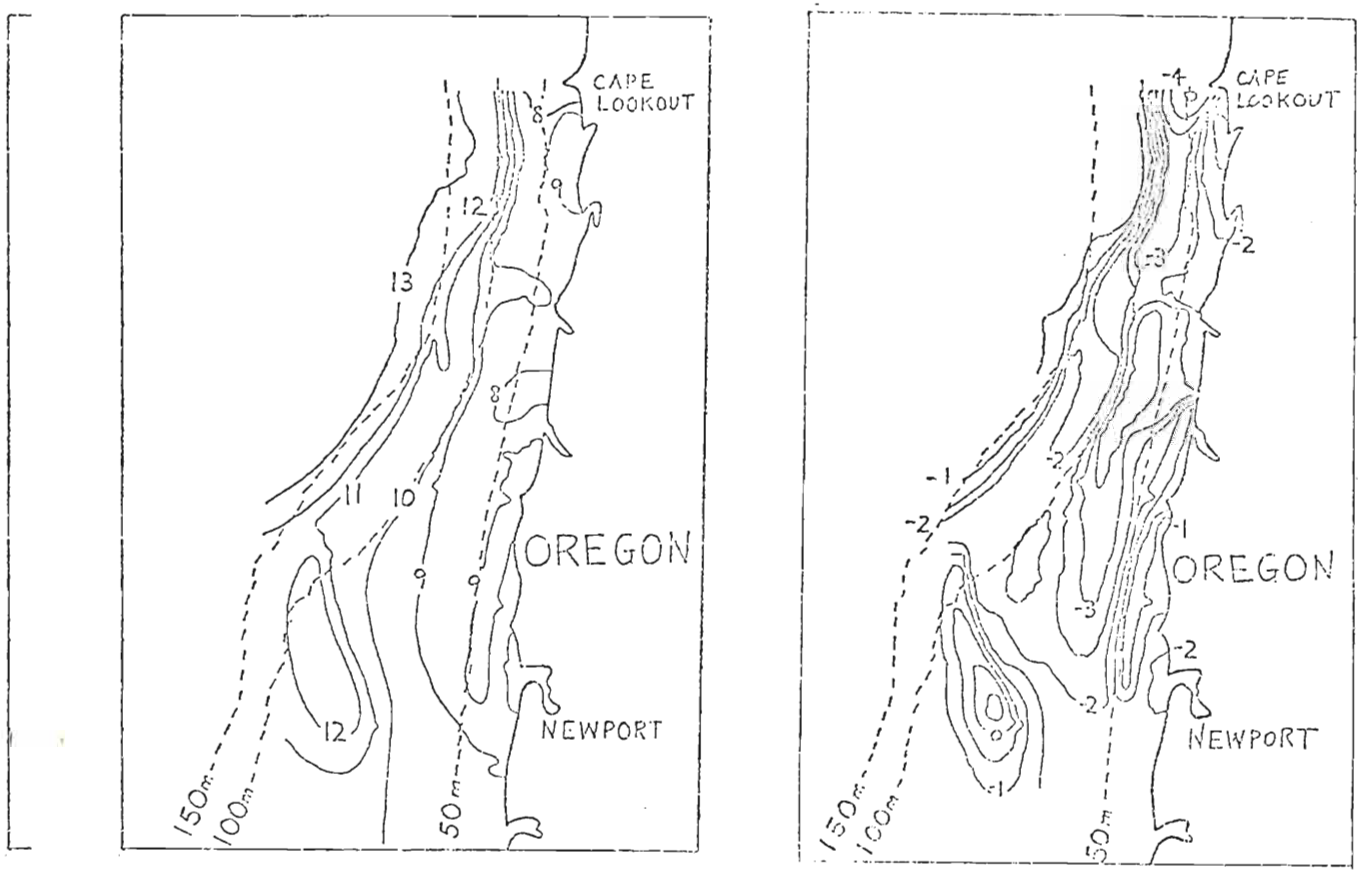

Fig. A-16. (a) Horizontal sea surface temperatures, and (b) perturbations from the three-week mean in the COHO flight region for 16 July, 1973.

REFERENCES

Bakun, A., 1972: The PEG upwelling index off Oregon during 1972. CUE Notes, 10, 8-12.

Bang, N. D., 1973: Characteristics of an intense ocean frontal system in the upwell regime west of Cape Town. Tellus, 25, 256-265.

Charney, J. G., 1971: Geostrophic turbulence. J. Atmos. Sci., 28, 1087-1095.

Cineca Newsletter, Published by The International Council for the Exploration of the Sea, Charlottenlund, Denmark, 1971.

Garvine, R. W., M.R. Stevenson, and B. Wyatt, 1974: Lagrangian measurements in a coastal upwelling zone off Oregon. (To be published in J. Phys. Oceanogr.)

Horn, L. H., and R. A. Bryson, 1963: An analysis of the geostrophic kinetic energy spectrum of large scale atmospheric turbulence. J. Geophys. Res., 68, 1059-1064.

Hurlburt, H. E., 1974: The influence of coastline geometry and bottom topography on the eastern ocean circulation. Ph.D. dissertation, Florida State University, Tallahassee.

Huyer, A., 1974: Observations of the coastal upwelling region off Oregon during 1972. Ph.D. dissertation, Oregon State University, Corvallis.

Johnson, A., and J. J. O'Brien, 1973: A study of an Oregon sea breeze event. J. Appl. Meteor., 12, 1267-1283.

Julian, P. R., W. M. Washington, L. Hembree, and C. Ridiley, 1970: On the spectral distribution of large-scale atmospheric kinetic energy. J. Atmos. Sci., 27, 376-387.

Kao, S. K., 1970: Wavenumber-frequency spectra of temperature in the free atmosphere. J. Atmos. Sci., 27, 1000-1007.

Kolmogorov, A. N., 1941: The local structure of turbulence in incompressible fluids for very large Reynold's numbers. Dokl. Akad. Nauk SSSR, 30, 301-305 (translation).

pressible fluids for very large Reynold's numbers. Dokl. Akad. Nauk SSSR, 30, 301-305 (translation).

Kraichnan, R., 1967: Inertial ranges in two dimensional turbulence. Physics Fluids, 10, 1417-1423.

Lilly, D. K., and P. F. Lester, 1974: Waves and turbulence in the stratosphere. J. Atmos. Sci., 31, 800-812.

MacLeish, W., 1970: Spatial spectra of ocean surface temperature. J. Geophys. Res., 75, 6872-6877.

Mooers, C. N. K., C. A. Collins, and R. L. Smith, 1973: The dynamic structure of the onset of a coastal upwelling event. (Submitted to J. Phys. Oceanogr.)

O'Brien, J. J., 1972: CUE-I Meteorological Atlas, Vol. I. Coastal upwelling ecosystems analysis, International Decade of Ocean Exploration, 319pp.

_____, 1972: Sea surface temperature changes. CUE Notes, 7, p.5.

_____, 1974a: The COHO Project (Living Resources Prediction Feasibility Study) Reports, Vol. I, Final Report, Oregon State University, Corvallis (Available from School of Oceanography, Oregon State University).

_____, 1974b: The COHO Project (Living Resources Prediction Feasibility Study) Reports, Vol. II, Environmental Report, Oregon State University, Corvallis (Available from School of Oceanography, Oregon State University).

_____, 1974c: The COHO Project (Living Resources Prediction Feasibility Study) Reports, Vol. III, System Evaluation Report, Oregon State University, Corvallis (Available from School of Oceanography, Oregon State University).

Richey, D., 1971: You can't catch Coho without KNOW-HOW. Sports Afield Fishing Annual, 1971 Ed., The Hearst Corp., 50-53.

Rossby, C. G., and collaborators, 1939: Relation between variations in intensity of the zonal circulation of the atmosphere and displacements of the semi-permanent centers of actions. J. Marine Res., 2, 38-55.

Ryther, J. H., 1969: Photosynthesis and fish production in the sea. Science, 166, 72-76.

Saunders, P. M., 1970: Corrections for airborne radiation thermometry. J. Geophys. Res., 75, 7596-7601.

Saunders, P. M., 1970: Corrections for airborne radiation thermometry. J. Geophys. Res., 75, 7596-7601.

_____, 1972: Space and time variability of temperature in the upper ocean. Deep Sea Research, 19, 467-480.

_____, and C. H. Wilkens, 1966: Precise airborne radiation thermometry. Proc. 4th Symposium Remote Sensing of Environment, Ann Arbor, Michigan, 815-826.

Smith, R. L., 1968: Upwelling. Oceanogr. Mar. Biol. Ann. Rev., 6, 11-47.

_____, 1974: A description of current, wind and sea level variation during coastal upwelling off the Oregon coast, July - August, 1972. J. Geophys. Res., 79, 435-443.

Thompson, J. D., 1973: Sea surface temperatures mapping of coastal upwelling areas using remote sensing. (Presented to the Coastal Upwelling Experimental Workshop, January 23, 1973, in Tallahassee, Florida.)

_____, 1974: The coastal upwelling cycle on a beta-plane: Hydrodynamics and thermodynamics. Ph.D. dissertation, Florida State University, Tallahassee.

Winn-Nielsen, A., 1967: On the annual variation and spectral distribution of atmospheric energy. Tellus, 19, 540-559.

VITA

Mr. Cleveland G. Holladay was born October 23, 1950, in North Platte, Nebraska. In 1972 he graduated from the Florida State University with a B.S. degree in Meteorology. He began his graduate study in the Department of Meteorology at the Florida State University in June 1972.